EXPERIMENTAL INSIGHTS INTO THE FORMATION OF HIGH-MG ANDESITES IN THE TRANS-MEXICAN VOLCANIC BELT

by

RACHEL MARIA WEBER

A THESIS

Presented to the Department of Geological Sciences
and the Graduate School of the University of Oregon
in partial fulfillment of the requirements
for the degree of
Master of Science

June 2010

"Experimental Insights into the Formation of High-Mg Andesites in the Trans-Mexican Volcanic Belt," a thesis prepared by Rachel Maria Weber in partial fulfillment of the requirements for the Master of Science degree in the Department of Geological Sciences. This thesis has been approved and accepted by:

Paul J. Wallace, Chair of the Examining Committee

6-1-10

Date

Committee in Charge: Dr. Paul J. Wallace, Chair
Dr. A. Dana Johnston
Dr. Eugene D. Humphreys

Accepted by:

Dean of the Graduate School

An Abstract of the Thesis of

Rachel Maria Weber for the degree of Master of Science in the Department of Geological Sciences to be taken June 2010

Title: EXPERIMENTAL INSIGHTS INTO THE FORMATION OF HIGH-MG ANDESITES IN THE TRANS-MEXICAN VOLCANIC BELT

Approved: _____
Paul J. Wallace

High-Mg basaltic andesites and andesites occur in the central Trans-Mexican Volcanic Belt, primarily in the region south of Mexico City, and their primitive chemical characteristics suggest equilibration with mantle peridotite. These lavas may represent either slab melts that re-equilibrated with peridotite during ascent or hydrous partial melts of a peridotite source. I have experimentally mapped the liquidus mineralogy for a high-Mg andesite from the Pelagatos cinder cone as a function of temperature and H_2O content over a range of mantle wedge pressures. The results concur with a published thermobarometer for peridotite melting and suggest that this composition could only be in equilibrium with a harzburgite residue at relatively high water contents and low pressures and temperatures. However, numerically adjusting the

composition for equilibrium with more refractory mantle (Fo_{92}) shifts these conditions to lower water contents and higher pressures and temperatures near where geodynamic models indicate peak mantle wedge temperatures.

CURRICULUM VITAE

NAME OF AUTHOR: Rachel Maria Weber

PLACE OF BIRTH: Marshfield, Wisconsin, USA

GRADUATE AND UNDERGRADUATE SCHOOLS ATTENDED:

University of Oregon, Eugene, OR
University of Washington, Seattle, WA
Shoreline Community College, Shoreline, WA

DEGREES AWARDED:

Master of Science, Geology, 2010, University of Oregon
Bachelor of Science, Earth and Space Sciences, 2008, University of Washington

AREAS OF SPECIAL INTEREST:

Geochemistry
Volcanology
Igneous Petrology

PROFESSIONAL EXPERIENCE:

Graduate Teaching Fellow, Department of Geological Sciences, University of Oregon, Eugene, OR, 2008-2010

Independent Undergraduate Research, University of Washington, Seattle, WA, 2007-2008

ACKNOWLEDGMENTS

I give my most sincere thanks to Professors Dana Johnston and Paul Wallace for their consistent generosity and insight throughout the research process and for their invaluable support in the preparation of this manuscript. I also thank Stephanie Weaver for her experimental guidance and incredibly helpful nature. I thank John Donovan for his analytical expertise and patience. I give thanks to Dr. Lorenzo Meriggi, who so kindly sent me the starting material for my experiments. I thank the National Science Foundation for granting me the funding to work on this project. And finally, I give thanks to my amazing family and friends for their constant support and good humor.

TABLE OF CONTENTS

Chapter Page

LIST OF FIGURES

LIST OF TABLES

CHAPTER I

INTRODUCTION

Overview

The overall goal of this project is to use hydrous, high-pressure rock-melting experiments to determine the P-T-X_{H2O} conditions at which a primitive high-Mg andesite from central Mexico could have been in equilibrium with mantle peridotite. The experimental results also provide constraints on the geodynamics of the mantle wedge overlying the subducting slab in this region. I present here an introduction to high-Mg andesites and the Trans-Mexican Volcanic Belt.

High-Mg Andesites

High-Mg andesites (HMAs) erupt in many volcanic arcs throughout the world, typically at convergent margins where young oceanic crust is being subducted. They are relatively uncommon, but their origin could provide insight into the formation of early continental crust on Earth (Tatsumi, 2006). HMAs have high MgO contents and Mg#s [=100 x molar[MgO/(MgO+FeO)] relative to typical andesitic arc magmas, and

their compositions are similar to that of the bulk continental crust (Tatsumi, 2006; Kelemen, 1995). Well-known examples include adakites from the Aleutian Islands (Crawford *et al.*, 1989), boninites from the Bonin Islands (Defant and Drummond, 1990), and the Setouchi andesites from Japan (Tatsumi, 2006). Adakites have high Sr/Y ratios and are depleted in heavy rare earth elements (HREE), whereas boninites are characterized by clinoenstatite phenocrysts (Tatsumi, 2006). The primitive chemical characteristics of HMAs suggest equilibration with mantle wedge peridotite; they may form either through shallow, wet partial melting of the mantle or through re-equilibration of slab melts migrating through the mantle wedge (Wood & Turner, 2009; Grove *et al.*, 2002; Kelemen, 1995).

Trans-Mexican Volcanic Belt

High-Mg andesites are found in the central Trans-Mexican Volcanic Belt (TMVB) in the Chichinautzin Volcanic Field (CVF) south of Mexico City (Figure 1). A combination of receiver function and tomographic images (Figure 2) from the Meso-American Subduction Experiment (MASE, Pérez-Campos *et al.*, 2008) show that this part of the volcanic arc has relatively thick crust (~40-50 km) and is associated with flat-slab subduction of the Cocos plate beneath the North American plate. The slab appears to ride flat along the base of the lithosphere for

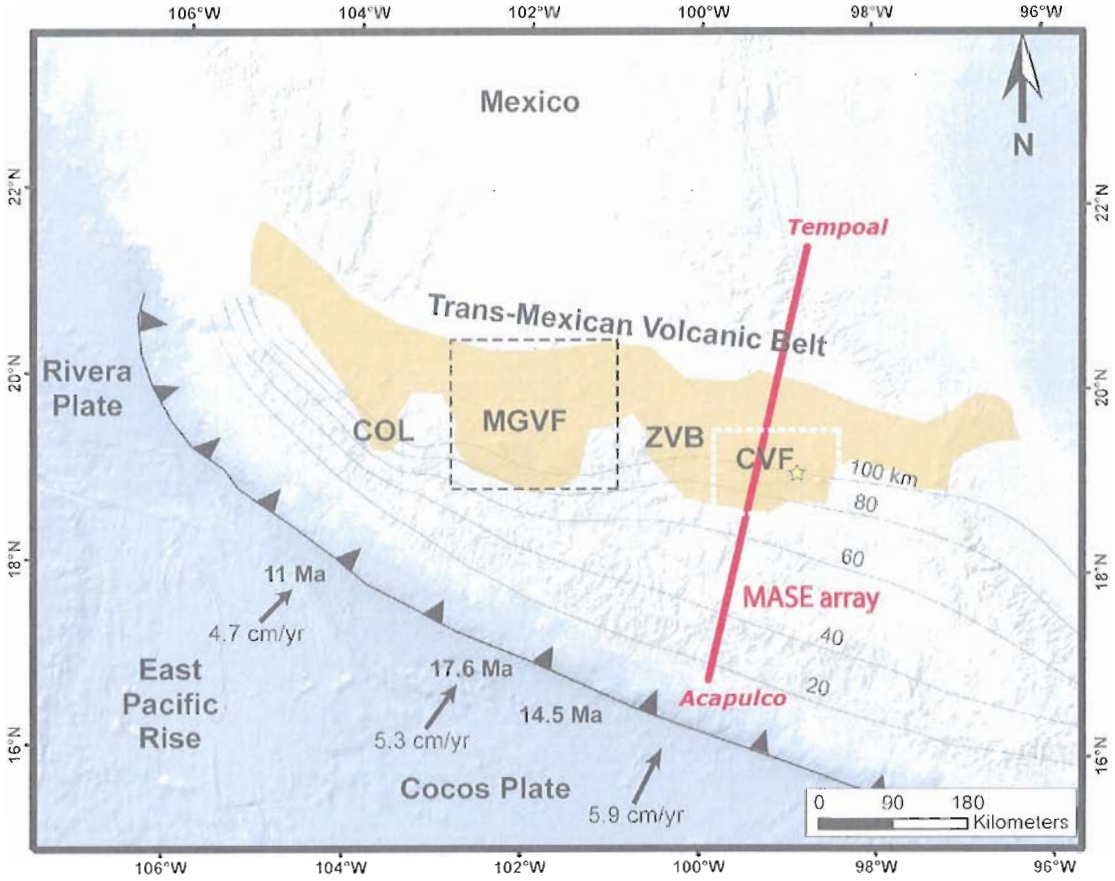

Figure 1. The Trans-Mexican Volcanic Belt (tan) and offshore plate boundaries. Location of MASE seismic array is shown in red (Pérez-Campos *et al.*, 2008). Ages of the subducting Cocos plate and slab isodepth contours are from Pardo & Suarez (1995). COL = Colima Volcano; MGVF = Michoacán-Guanajuato Volcanic Field; ZVB = Zitácuaro-Valle de Bravo volcanic field; CVF = Chichinautzin Volcanic Field. Pelagatos cinder cone is the yellow star (Guilbaud *et al.*, 2009; Meriggi, *et al.*, 2008; Schaaf *et al.*, 2005). Figure is modified from Johnson *et al.* (2009).

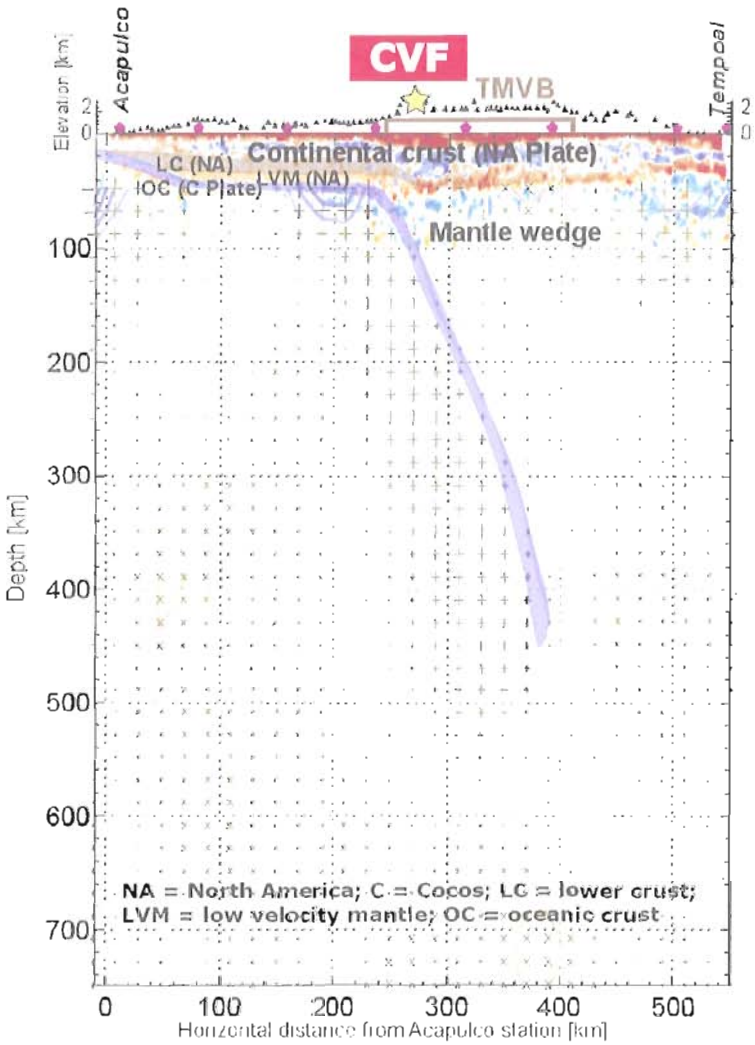

Figure 2. Composite of receiver function and tomographic images from the Meso-American Subduction Experiment (MASE) showing the flat and descending areas of the Cocos plate. Black triangles denote the position of broadband stations. Purple symbols are major cities along the MASE transect. Brown line denotes the extent of the TMVB (Pérez-Campos *et al.*, 2008). Location of CVF is shown below the red bar. Pelagatos cinder cone (yellow star) is located ~40 km east-southeast of this transect. Figure is modified from Pérez-Campos *et al.* (2008).

~300 km and then plunges into the asthenosphere at ~65° beneath the volcanic arc (Manea and Manea, in review).

The CVF is a 2,400 km^2 volcanic field bounded on the east by the Sierra Nevada and on the west by Nevado de Toluca (Meriggi *et al.*, 2008). It is made up of >200 monogenetic cinder cones and shield volcanoes ranging in composition from basalt to dacite. CVF lavas are chemically heterogeneous, including calc-alkaline and ocean island basalt (OIB) type lavas. In the CVF, lavas have generally higher MgO contents at a given value of SiO_2 than elsewhere in the TMVB, as shown in Figure 3 (Wallace & Carmichael, 1999).

The Pelagatos cinder cone produced the most primitive known lava in the CVF less than 14,000 years ago (Guilbaud *et al.*, 2009). It is located ~20 km southeast of Mexico City and ~30 km west-northwest of Popocatépetl. It is composed of one main scoria cone and two scoria ridges, as well as a lava flow that is 7 km long and 0.5-1 km wide with a bulk volume of ~40,000,000 m^3 (Guilbaud *et al.*, 2009). Beneath it, the crust appears to be 40-50 km thick, based on the receiver function image in Figure 2, with the top of the subducting slab at ~100 km depth.

The Pelagatos lava (analysis in Table1, Chapter II) is a high-Mg basaltic andesite containing 54.0 wt% SiO_2 and 9.2 wt% MgO; it has an Mg# of 75.8 (FeO/FeO_T=0.76; calculated using Kress & Carmichael, 1991; oxygen fugacities from Wallace & Carmichael, 1999) and is in

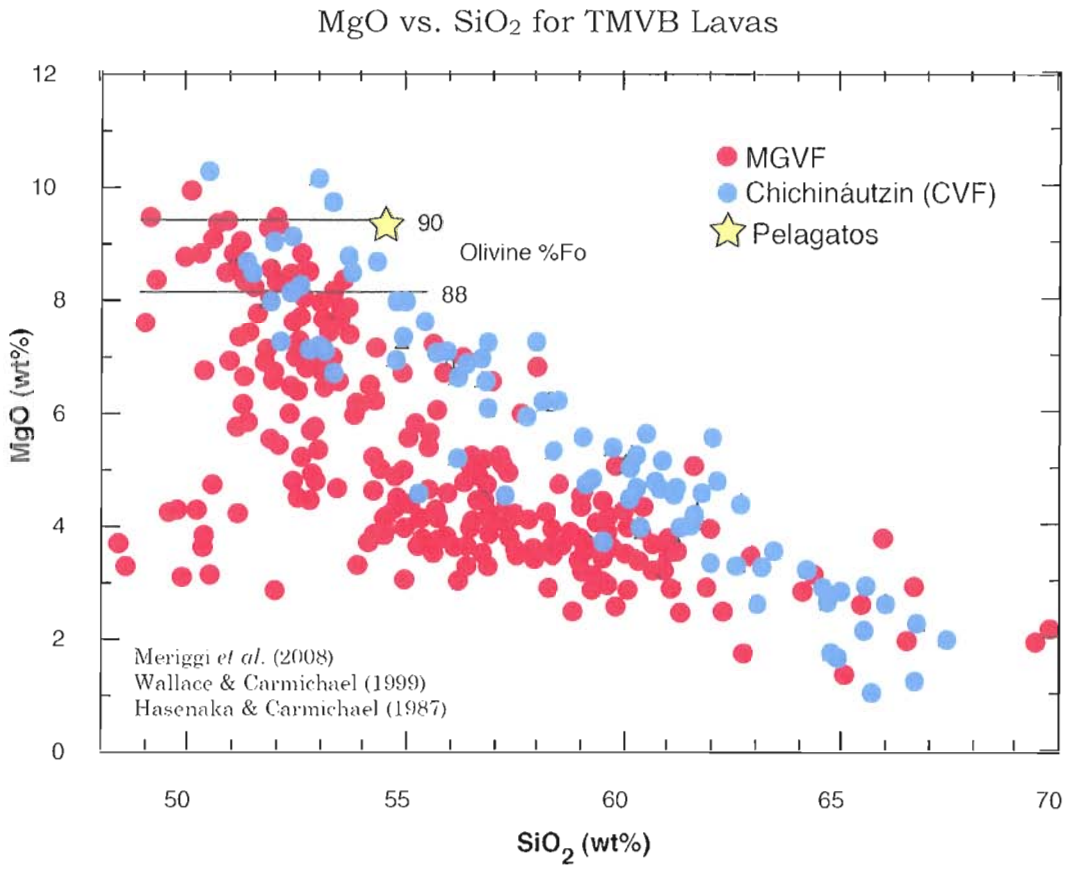

Figure 3. Comparison of MgO vs. SiO_2 for the CVF (blue) and the Michoacán-Guanajuato Volcanic Field (MGVF, red) showing the elevated MgO content relative to SiO_2 in CVF lavas (Wallace & Carmichael, 1999). Yellow star denotes the Pelagatos bulk composition (normalized to 100% anhydrous). It is in equilibrium with $Fo_{90.7}$ olivine.

equilibrium with $Fo_{90.7}$ olivine (Meriggi *et al.*, 2008; Schaff *et al.*, 2005). The Pelagatos bulk $^{87}Sr/^{86}Sr$ (.70410) and ε_{Nd} (4.1) are approximately average for the CVF (Meriggi *et al.*, 2008). The lava has characteristics

common to other high-Mg andesites, such as enrichment in compatible trace elements (Ni and Cr) and Cr-spinel inclusions in Mg-rich olivine (~Fo_{88}) phenocrysts (Guilbaud *et al.*, 2009; Meriggi *et al.*, 2008; Tatsumi & Ishizaka, 1982). It is aphyric to porphyritic with phenocrysts of euhedral olivine and cpx, and plagioclase microlites in the groundmass (Guilbaud *et al.*, 2009).

Wet Mantle Melting vs. Re-equilibration of Slab Melts

The notably primitive composition of the Pelagatos lava suggests it was generated by hydrous partial melting of an ultramafic (harzburgite or lherzolite) source or by re-equilibration of a deep ascending slab-derived melt with peridotite. Geodynamic models by van Keken *et al.* (2002), Kelemen *et al.* (2003), and Peacock (2003) predict that low temperatures could exist at great depth in the upper mantle and altered oceanic crust of the subducting plate, which transports water to the mantle in the form of hydrous minerals. As hydrated oceanic lithosphere sinks into the mantle, high temperatures and pressures dehydrate these minerals and release H_2O-rich fluids and/or silicate melt into the overlying mantle. Whether dehydration reactions produce a fluid or slab-melt is a function of both the age of the subducting crust and the speed of subduction (van Keken *et al.*, 2002).

On one hand, H_2O-rich fluids could have risen and hydrated the mantle wedge, lowering its solidus temperature and producing magma by fluid-fluxed melting (Grove *et al.*, 2006; Parman & Grove, 2004; Grove *et al.*, 2003; Wallace & Carmichael, 1999). This process is best described by the model shown in Figure 4, illustrating the inverted thermal gradient created by corner flow in the mantle wedge (Grove *et al.*, 2003), which is induced by the coupling of the mantle to the cold subducting slab. This type of melting is a likely process for the formation of the Pelagatos magma because its minimum pre-eruptive magmatic H_2O content is ~3 wt% based on FTIR analyses of olivine-hosted melt inclusions (J. Roberge, unpublished data). For other TMVB lavas, H_2O contents as high as 5 wt% have been found (Cervantes & Wallace, 2003). In addition, high-Mg andesites have been experimentally produced by the water-saturated melting of peridotite (Hirose, 1997), confirming that the Pelagatos lava could have been produced by hydrous partial melting of mantle.

On the other hand, the subducting slab beneath central Mexico is very young, so it is hotter than average, possibly hot enough to release silicate melt into the mantle. H_2O-rich, approximately dacitic melts from the amphibolitic/eclogitic crustal section of the subducting slab could have interacted with mantle peridotite to form orthopyroxene at the expense of olivine (Straub et al., 2008). As such slab melts percolated

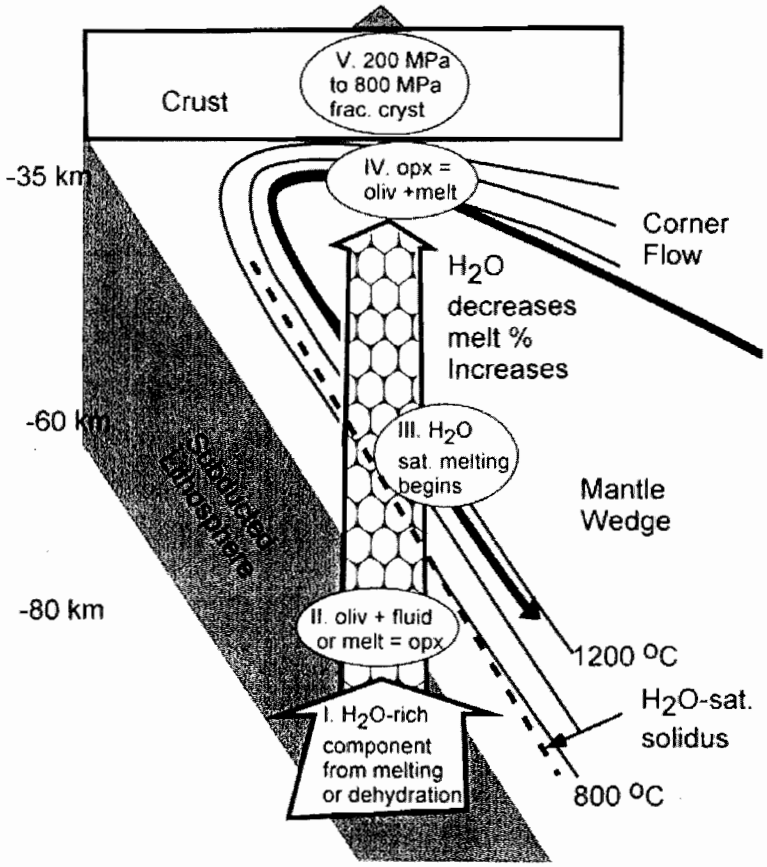

Figure 4. Model of melt generation in the mantle wedge (Grove et al., 2003). I) H_2O-rich component produced from dehydration of minerals in the subducted lithosphere. II) H_2O-rich component ascends into the mantle wedge, where it is stripped of SiO_2. III) Fluid-rich component ascends into shallower, hotter mantle that exceeds the vapor-saturated solidus of peridotite and melting begins. IV) Melting takes place by reactive porous flow (Gaetani & Grove, 2003; Grove *et al.*, 2002) and continues into the shallow mantle wedge, where the melt dissolves opx and precipitates olivine. V) Magma reaches the overlying crust.

upward through the mantle wedge and this peritectic reaction occurred, the melts would re-equilibrate with the overlying mantle assemblage prior to ascent through the crust. The contribution of the slab-derived melt would be discernable in the geochemical characteristics of the erupted lavas, such as low overall HFSEs (high field-strength elements) and MREE-HREEs (medium and heavy rare earth elements), low Nb/Ta ratios, and high SiO_2 contents (Gomez-Tuena *et al.*, 2007).

In the following section, I describe and discuss a set of hydrous, high-pressure, near-liquidus experiments performed using lava from the Pelagatos cinder cone. These experiments can be used to map the H_2O-undersaturated liquidus surface for the Pelagatos composition and place constraints on the pressure, temperature, and H_2O contents of the mantle wedge beneath central Mexico. I also discuss a method for monitoring fO_2 in rock-melting experiments involving mafic melt in equilibrium with $Au_{75}Pd_{25}$ capsules.

CHAPTER II

METHODS

Overview

The experiments described here utilized two end-loaded piston-cylinder apparatuses in the Experimental Petrology Laboratory at the University of Oregon. Anhydrous phase relations were estimated using the MELTS and pMELTS models (Ghiorso *et al.*, 2002), and hydrous phase relations were determined experimentally using finely ground, natural rock starting materials. These materials were enclosed with variable amounts of distilled water in $Au_{75}Pd_{25}$ capsules, which were sealed by arc welding.

Because the Pd component of these capsules readily alloys with Fe from the partially to completely molten rock, it was necessary to presaturate the capsules with Fe. This presaturation procedure was performed using a Deltec VT-31 1-atm gas-mixing furnace. A method was also developed whereby this Fe-presaturation was used to impose a desired oxygen fugacity (fO_2) during the subsequent hydrous, high-

pressure experiments. Experimental methods and analytical procedures used in this work are described in the following sections in detail.

Starting Materials and Compositions

The starting materials for my experiments were natural basalts and basaltic andesites: a MORB, SO-12-88-D2 (Hebert *et al.*, 1983), and two subduction-related Mexican basaltic andesites, JR-28 (J. Roberge, unpublished data) and d-25 (Meriggi *et al.*, 2008). These samples were provided by Dr. Dana Johnston, Stephanie Weaver, and Dr. Lorenzo Meriggi, respectively. The powders were ground under ethanol to <10 microns. Their bulk compositions are given in Table 1.

One Atmosphere Experiments

To calibrate the relationship between the prevailing fO_2 of the piston-cylinder experiments and the amount of Fe lost to the AuPd capsules, eighteen rock-melting experiments (RMW prefixes, Table 2, Chapter III) were performed in a gas-mixing furnace at 1 atm using the three previously described mafic rock compositions: a MORB (9.4 wt% FeO_T) and two subduction-related Mexican basaltic andesites (7.6 wt% and 6.9 wt% FeO_T). Approximately 30 mg of each powder was packed into individual $Au_{75}Pd_{25}$ capsules. Capsules were triple-crimped and welded on the bottom, but left open on top. The samples were run for

Table 1. Starting Compositions

	SO-12-88-D2	JR-28[b]	d-25[b]
SiO_2	49.82	52.72	54.00
TiO_2	1.43	0.76	0.81
Al_2O_3	15.76	16.05	15.42
FeO_T	9.38	7.57	6.91
MnO	0.10	0.13	0.12
MgO	8.66	9.35	9.24
CaO	11.13	8.34	7.51
Na_2O	2.45	3.39	3.35
K_2O	0.05	0.78	0.96
P_2O_5	-	0.15	0.15
Total	98.78	99.24	98.47
Mg#[a]	62.2	74.3	75.8

X-ray fluorescence analyses given in wt%

[a] Mg# = 100 x molar[MgO/(MgO+FeO)]

[b] FeO/FeO_T=0.76 (Kress & Carmichael, 1991)

48-72 hours in a Deltec VT-31 1-atm gas-mixing vertical quench furnace at 1200°C and 1300°C and three different oxygen fugacities spanning from -1 to +2 log units relative to the nickel-nickel oxide (NNO) buffer (Huebner & Sato, 1970).

Experimental oxygen fugacities were controlled with CO_2/H_2 gas mixtures and measured with a ZrO_2-based solid electrolyte fO_2 sensor using platinum electrodes and breathable grade air as a reference gas.

Temperatures were measured with a $Pt/Pt_{10}Rh$ thermocouple that had been previously calibrated against the melting point of Au. Three of the experiments had to be repeated, due to a tendency for the melt to creep up and over the edge of the capsule at 1200°C and fO_2=NNO-1. All samples were drop-quenched into a bulb of cool water to ensure rapid quenching. Experimental run products were mounted in epoxy, cut in half, polished to ¼ μm, and carbon coated for examination on the scanning electron microscope (SEM) and analysis on the electron probe microanalyzer (EPMA).

Presaturation of AuPd Capsules

To reduce iron loss from the experimental melts to AuPd capsules in my piston-cylinder experiments (RW prefixes, Table 4, Chapter III), I presaturated 25 $Au_{75}Pd_{25}$ capsules with Fe prior to re-using them in high-P experiments. For each capsule presaturation, I packed ~30 mg of ground Pelagatos lava powder (d-25, Table 1) into a $Au_{75}Pd_{25}$ capsule. Capsules were triple-crimped and welded closed on the bottom, but left open on top. Samples were melted in the 1-atm gas-mixing furnace at 1300°C and fO_2 of NNO-0.4 for ~48 hours.

The eventual goal was to run high-P experiments at NNO+0.6, the approximate intrinsic fO_2 of the d-25 starting composition (based on analyses of CVF lavas by Wallace & Carmichael, 1999). Therefore, my

aim here was to dissolve into the AuPd capsules an amount of Fe that would be in equilibrium with a melt of the Pelagatos composition at this fO_2. However, had I simply run these presaturation runs at an fO_2 of NNO+0.6, the result would have been an alloy with the correct Fe content for equilibrium with d-25 *after it lost Fe to the capsules*, which would be too low a concentration to be in equilibrium with the sample containing its full complement of Fe. To raise the concentration to a more appropriate value, the presaturation runs were performed at an fO_2 one log unit more reducing (NNO-0.4) than the final desired fO_2 to increase the activity of Fe° in the melt, causing more to dissolve into the AuPd capsules. This shift of one log unit has been previously shown by Médard *et al.* (2008) to approximately compensate for this effect. As will be discussed in Chapter III, it turns out that this shift slightly overcompensated, leading to Fe-gain (<10 relative %) in the sample for most near-liquidus runs (Figure 10, Chapter III).

To quench these runs, I extracted the presaturated capsules through the top of the furnace and allowed them to cool to room temperature in air, which occurred quickly enough to prevent any significant change in the Fe-content of the Fe-Au-Pd alloy. The glass was removed from the capsules by drilling it out with a diamond bit to remove as much as possible. The remaining glass was dissolved by heating the capsules in hydrofluoric acid for ~72 hours at 50°C in a sealed Teflon

digestion bomb on a hot plate. Finally, I cleaned the presaturated capsules in deionized water and then ethanol in an ultrasonic bath to remove any residual fluorides. These Fe-presaturated capsules were then re-used in subsequent high-pressure piston-cylinder experiments.

Piston-Cylinder Experiments

To determine the water-undersaturated liquidus phase relations of the Pelagatos lava starting material, I performed twenty-one hydrous piston-cylinder experiments. Approximately 20 mg of the finely ground (<10 μm) Pelagatos powder was packed into Fe-presaturated $Au_{75}Pd_{25}$ capsules. Each capsule was weighed (precision of ~0.1 mg) before and after the powder was loaded to determine the mass of the powder. I then calculated the mass of water needed for each run to achieve the desired nominal water content (3, 5, or 7 wt%) and loaded this amount of deionized water into the capsule using a 1.0 μL microsyringe (precision of ~0.1 mg).

Next, I weighed each capsule to establish the actual amount of water that had been loaded. I then crimped and snipped the capsule and weighed it again before placing it between the Cu jaws of a small vice, while submerging the bottom in a cool water bath to prevent water volatilization upon welding. After welding the top of each capsule, I then reweighed them to ensure no water was lost. CaF_2/MgO-based furnace

assemblies, described by Pickering *et al.* (1998), were used in all experiments in a ½" end-loaded piston-cylinder apparatus. The pre- and post-run sample positions were measured to ensure that the capsule and thermocouple were within the hot spot of the furnace, as previously mapped with double thermocouples by Pickering *et al.*, (1998).

Experiments were run at 7, 10, 12, 13, 14, 15, and 20 kbar, and Heise gauge pressures were maintained to within ~100 psi of the nominal target P, equivalent to ±~0.5 kbar sample pressure. Samples were pressurized at room temperature and then heated to the target temperature (1140 to 1345°C). Temperatures were maintained within ~5°C of the target using Eurotherm 808 temperature controllers and $W_5Re/W_{26}Re$ thermocouples. Run durations ranged from 12.5 to 18 hours, guided by a desire to achieve equilibrium in these melt-rich runs, while also minimizing H_2O loss from the capsule. Experiments were quenched by cutting power to the piston-cylinder and allowing it to cool to subsolidus temperatures in ~2 seconds. Run products were mounted in epoxy, cut in half to show a gravity section, polished to ¼ μm, and carbon coated for SEM/EPMA analysis.

SEM and EPMA Analyses

The experimental run products were analyzed at the CAMCOR MicroAnalytical Facility at the University of Oregon. Backscattered

electron images were acquired using a FEI Quanta SEM to evaluate mineral identities, modes, and sample textures. Qualitative elemental analyses were performed using energy dispersive x-ray spectroscopy (EDS). Quantitative chemical analyses were obtained with a Cameca SX-100 electron microprobe using different instrument set-ups optimized for chemical analysis of 1) hydrous glasses 2) crystalline mineral phases, and 3) capsule alloys.

The hydrous glasses were analyzed using a 15 kV accelerating voltage, a 20 nA beam current, and a 10 μm spot size to minimize Na migration from the beam. All experiments were run at near-liquidus temperatures, so finding suitably large areas of glass for these broad beam analyses was not a problem. Minerals were analyzed using a 15 kV accelerating voltage, a 20 nA beam current, and a focused beam (<1μm), due to their usual small crystal size (<5 μm). Finally, capsule alloys were analyzed using a 20 kV accelerating voltage, 30 nA beam current, and a focused beam.

Natural and synthetic minerals, glasses, and pure metals were used as standards for these analyses. A correction was applied to account for Na-loss in the glass analyses (Nielsen & Sigurdsson, 1981), and H_2O was estimated using the water-by-difference method, calibrated by Roman *et al.* (2006). These options are both available in the Probe for EPMA software that was used.

CHAPTER III

RESULTS

Overview

In this section, I present the results from both one-atmosphere experiments and high-pressure piston-cylinder experiments. The former provided a calibration that enabled me to constrain the fO_2 in water-undersaturated piston-cylinder rock-melting experiments by monitoring the Fe content of (Fe)AuPd alloy capsules after the runs. The high-pressure experiments generated products that allowed me to map the liquidus mineralogy onto the water-undersaturated liquidus surface for the Pelagatos composition. These results also provide constraints on the depth and temperature at which a hydrous melt with the Pelagatos composition (d-25, Table 1) could have been in equilibrium with an upper mantle mineral assemblage.

fO_2 Calibration for (Fe)AuPd Alloys

After analyzing the melts and capsules from the one-atmosphere experiments for Fe using the electron microprobe (EPMA results given in

Tables 3 and 4), Fe partition coefficients (D_{Fe}) were calculated by dividing the mole fraction of Fe in the capsule by the mole fraction of FeO in the melt (Table 2). These partition coefficients are strong functions of both temperature and oxygen fugacity. Three experiments were discarded due to unacceptable Fe-gradients in the capsule materials, indicating that 48 hours was not long enough for Fe-rich compositions to attain equilibrium in these runs (Table 2, Figure 5).

Table 2. Conditions and Results of Fe-Partitioning Experiments

Run	FeO_T[a]	T (°C)	fO_2	Dur.	$X_{Fe}^{Capsule}$	X_{FeO}^{Melt}	D_{Fe}
RMW-1	9.4	1300	NNO-1	48 h	0.0351(8)	0.0416(11)	0.844(28)
RMW-2	7.6	1300	NNO-1	48 h	0.0262(4)	0.0274(9)	0.956(34)
RMW-3	6.9	1300	NNO-1	48 h	0.0266(3)	0.0289(7)	0.923(23)
RMW-4	9.4	1300	NNO+2	48 h	0.0043(3)	0.0804(8)	0.053(3)
RMW-5	7.6	1300	NNO+2	48 h	0.0038(3)	0.0599(8)	0.063(6)
RMW-6	6.9	1300	NNO+2	48 h	0.0043(6)	0.0585(8)	0.074(10)
RMW-7	9.4	1200	NNO-0.4	48 h	0.0247(8)	0.0709(8)	0.349(11)
RMW-8	7.6	1200	NNO-0.4	48 h	0.0147(1)	0.059(11)	0.248(5)
RMW-9	6.9	1200	NNO-0.4	48 h	0.0121(3)	0.0541(8)	0.224(7)
RMW-10	9.4	1300	NNO-0.4	48 h	0.0322(4)	0.0488(4)	0.659(10)
RMW-11	7.6	1300	NNO-0.4	48 h	0.0262(4)	0.0356(4)	0.735(15)
RMW-12	6.9	1300	NNO-0.4	48 h	0.0249(1)	0.0340(7)	0.734(16)
RMW-13	9.4	1200	NNO-1	72 h	0.0520(3)	0.0509(2)	1.023(8)
RMW-14	7.6	1200	NNO-1	72 h	0.0265(1)	0.0421(5)	0.630(8)
RMW-15	6.9	1200	NNO-1	72 h	0.0208(7)	0.0302(4)	0.689(26)
RMW-16	9.4	1200	NNO+2	48 h	0.0069(0)	0.0869(8)	0.080(1)
RMW-17	7.6	1200	NNO+2	48 h	0.0064(6)	0.0859(8)	0.075(7)
RMW-18	6.9	1200	NNO+2	48 h	0.0054(6)	0.0583(6)	0.094(11)

Run labels in bold denote experiments not considered in regression due to steep Fe-gradients in capsule alloys; numbers in parentheses next to each analysis represent 1σ standard deviation; errors given in terms of least unit cited [e.g., 0.0351(8) represents 0.0351 ± 0.0008]

[a] All runs with 9.4 wt% FeOT used SO-12-88-D2 starting material; 7.6 wt% FeOT used JR-28; 6.9 wt% FeOT used d-25; starting material analyses given in Table 1

Table 3. Electron Microprobe Analyses of One-Atm Glasses

Run	SiO_2	TiO_2	Al_2O_3	Cr_2O_3	FeO_T[a]	MnO	MgO	CaO	Na_2O	K_2O	P_2O_5	Total
RMW-1 (*n*=10)	51.72(27)	1.31(5)	15.40(18)	0.10(1)	4.94(13)	0.17(2)	12.57(30)	11.32(28)	2.33(7)	0.09(0)	0.11(1)	100.06(29)
RMW-2 (10)	55.44(20)	0.80(3)	17.81(5)	0.08(2)	3.18(10)	0.12(2)	9.76(4)	8.74(22)	3.50(10)	0.83(1)	0.14(1)	100.41(33)
RMW-3 (10)	56.54(29)	0.86(3)	16.50(11)	0.09(2)	3.38(8)	0.13(2)	10.15(6)	8.01(13)	3.59(7)	1.00(1)	0.15(1)	100.40(42)
RMW-4 (9)	48.43(32)	1.21(3)	14.50(9)	0.08(2)	9.40(9)	0.18(2)	12.26(5)	10.55(16)	2.20(8)	0.08(0)	0.08(2)	98.70(33)
RMW-5 (6)	52.49(17)	0.73(2)	16.78(14)	0.05(1)	6.79(9)	0.14(2)	9.06(6)	8.15(13)	3.37(14)	0.79(1)	0.13(1)	98.49(25)
RMW-6 (10)	54.08(12)	0.80(3)	15.65(9)	0.07(2)	6.74(9)	0.12(1)	9.68(3)	7.57(13)	3.48(16)	0.96(0)	0.14(2)	99.29(40)
RMW-7 (5)	51.25(38)	1.71(3)	14.97(12)	0.06(2)	8.20(10)	0.20(1)	8.17(5)	12.58(25)	2.63(10)	0.10(0)	0.11(1)	99.99(50)
RMW-8 (6)	55.43(22)	0.98(2)	16.94(10)	0.02(1)	6.79(12)	0.14(1)	6.78(9)	8.77(20)	3.95(21)	0.98(2)	0.17(1)	100.70(40)
RMW-9 (8)	56.09(17)	0.93(4)	17.13(14)	0.03(1)	6.22(9)	0.13(2)	6.82(6)	8.58(16)	3.93(7)	1.03(0)	0.16(0)	101.06(28)
RMW-10 (10)	51.36(18)	1.32(3)	15.40(8)	0.11(2)	5.84(4)	0.16(2)	12.90(6)	11.31(14)	2.26(10)	0.09(1)	0.09(1)	100.84(27)
RMW-11 (10)	55.57(24)	0.79(2)	17.74(12)	0.10(2)	4.15(5)	0.12(1)	9.43(4)	8.68(14)	3.46(8)	0.84(1)	0.14(1)	101.03(20)
RMW-12 (10)	56.60(28)	0.85(3)	16.44(10)	0.09(1)	3.98(9)	0.12(1)	9.94(5)	8.06(15)	3.51(8)	1.02(1)	0.15(1)	100.76(24)
RMW-13 (7)	53.20(22)	1.87(16)	15.02(14)	0.06(2)	5.82(5)	0.18(1)	8.03(5)	11.58(17)	2.75(7)	0.13(0)	0.18(1)	98.83(40)
RMW-14 (7)	56.53(65)	0.98(8)	16.49(16)	0.04(1)	4.77(14)	0.16(1)	6.68(12)	8.57(29)	3.91(11)	0.98(3)	0.25(1)	99.35(52)
RMW-15 (7)	58.53(80)	0.89(7)	16.67(15)	0.05(2)	3.42(22)	0.12(2)	6.31(18)	8.05(36)	4.09(23)	1.18(5)	0.24(1)	99.55(56)
RMW-16 (9)	50.06(17)	1.62(3)	14.67(9)	0.04(1)	9.93(9)	0.19(1)	7.96(3)	11.87(20)	2.56(10)	0.10(0)	0.11(2)	99.26(21)
RMW-17 (9)	54.18(28)	0.95(5)	17.17(82)	0.04(2)	9.93(9)	0.14(2)	6.56(32)	8.45(43)	3.860(10)	0.98(5)	0.16(1)	99.82(46)
RMW-18 (9)	55.22(30)	0.91(3)	17.07(17)	0.02(1)	6.60(7)	0.13(2)	6.57(12)	8.30(11)	3.79(16)	1.07(1)	0.17(1)	99.85(53)

Microprobe analyses in wt%; numbers in parentheses next to each analysis represent 1σ standard deviation on average of multiple analyses; errors given in terms of least unit cited [e.g., 51.72(27) represents 51.72 ± 0.27]

n number of analyses

[a] All Fe reported as FeO_T

Table 4. Electron Microprobe Analyses of One-Atm Capsule Alloys

Run	Fe wt%	Au wt%	Pd wt%	Mn wt%	Ni wt%	Total
RMW-1 (*n*=2)	1.25(3)	70.10(51)	27.54(71)	*MDL*	0.01(0)	98.91(27)
RMW-2 (2)	0.92(2)	70.36(8)	27.54(59)	0.01(1)	*MDL*	98.84(47)
RMW-3 (2)	0.94(1)	70.49(117)	27.68(35)	*MDL*	0.02(1)	99.12(82)
RMW-4 (2)	0.15(1)	70.94(3)	26.70(10)	*MDL*	*MDL*	97.78(6)
RMW-5 (2)	0.13(1)	71.80(13)	27.16(7)	*MDL*	*MDL*	99.09(23)
RMW-6 (2)	0.15(2)	71.95(2)	27.48(13)	*MDL*	0.02(1)	99.60(13)
RMW-7 (2)	0.87(3)	70.26(62)	27.28(65)	*MDL*	*MDL*	98.40(1)
RMW-8 (2)	0.52(0)	71.19(51)	27.4(54)	0.01(0)	0.01(1)	99.21(3)
RMW-9 (2)	0.43(1)	71.80(63)	27.43(19)	0.01(1)	*MDL*	99.6(44)
RMW-10 (2)	1.13(1)	69.99(10)	26.89(23)	*MDL*	0.01(3)	98.01(29)
RMW-11 (2)	0.92(2)	70.84(18)	27.22(51)	*MDL*	0.02(1)	99.00(30)
RMW-12 (2)	0.88(0)	70.64(44)	27.30(30)	0.02(0)	0.02(2)	98.86(16)
RMW-13 (2)	1.90(1)	72.38(60)	26.83(24)	*MDL*	0.04(0)	101.15(83)
RMW-14 (2)	0.96(0)	72.39(22)	28.17(15)	*MDL*	*MDL*	101.50(36)
RMW-15 (2)	0.75(3)	72.42(6)	28.07(12)	*MDL*	0.03(1)	101.26(12)
RMW-16 (2)	0.24(0)	70.79(8)	26.94(15)	*MDL*	0.01(1)	97.96(27)
RMW-17 (2)	0.22(2)	70.96(1)	26.93(32)	*MDL*	0.02(0)	98.13(29)
RMW-18 (2)	0.19(2)	71.09(51)	26.88(1)	*MDL*	*MDL*	98.16(53)

Microprobe analyses given here include only the first two analyses for each run in the appendix; numbers in parentheses next to each analysis represent 1σ standard deviation on average of multiple analyses; errors given in terms of least unit cited [e.g., 1.25(3) represents 1.25 ± 0.03]

n number of analyses, *MDL* below minimum 99% detection limit

Oxygen fugacity controls the Fe^{3+}/Fe^{2+} ratio of magma, and thus variations in oxygen fugacity can have important effects on mineral stability during magma crystallization. For basaltic glasses and volcanic rock samples, fO_2 can be estimated by measuring Fe_2O_3 and FeO (e.g., Christie *et al.*, 1986). Another commonly used technique (e.g., Parkinson & Arculus, 1999) is to measure the compositions of coexisting mineral

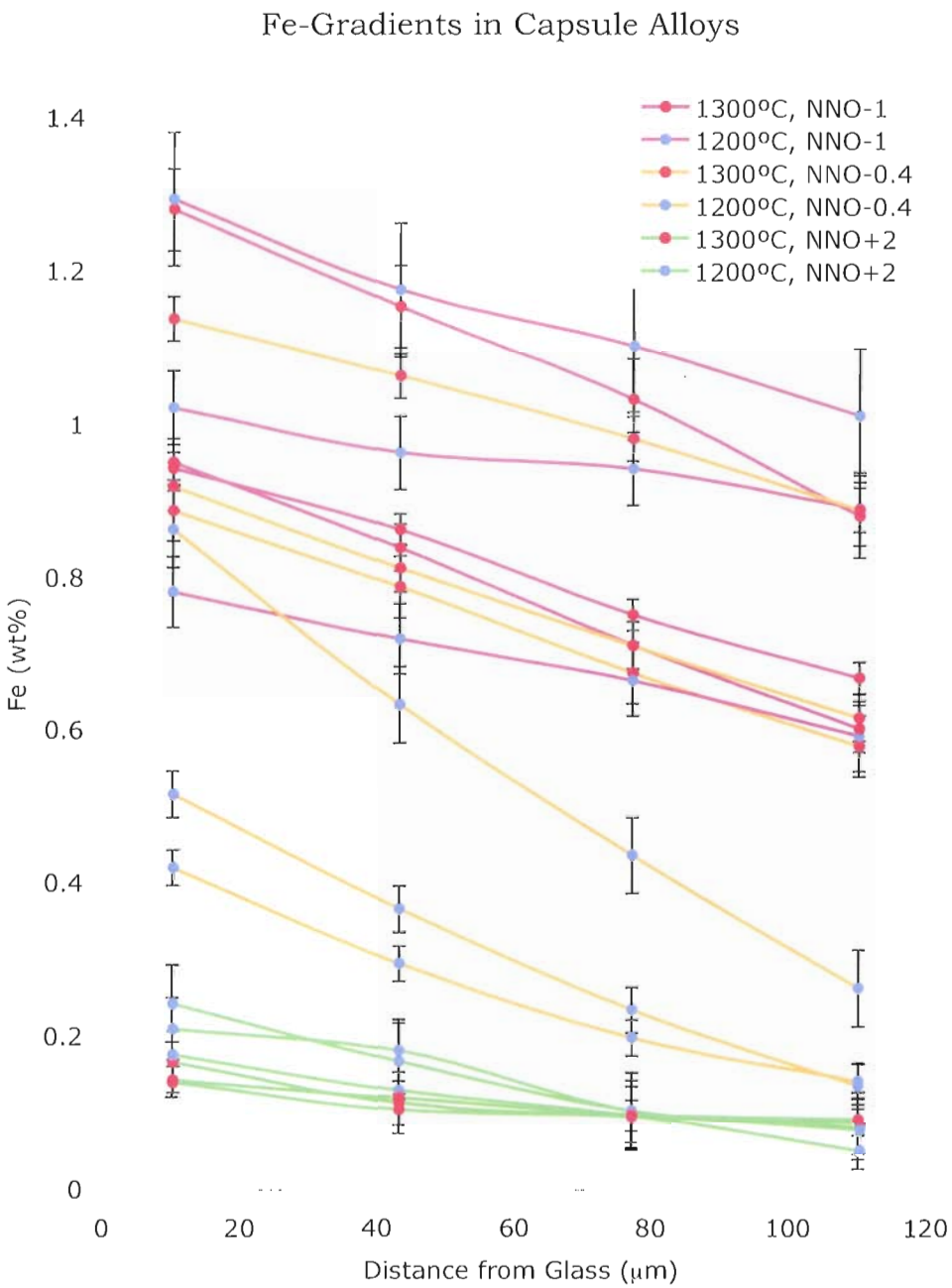

Figure 5. Fe-gradients in capsule alloys through ~100μm of capsule material adjacent to melts. Error bars represent 2σ. Discarded runs (1200°C and NNO-0.4) were deemed insufficiently equilibrated, based on relatively steep gradients in Fe content over this 100μm transect.

phases to calculate fO_2. Based on these methods, the fO_2 of arc magmas ranges from the fayalite-magnetite-quartz buffer (FMQ) to 2 log units more oxidizing than FMQ (FMQ+2). This fO_2 is generally more oxidizing than for MORB (FMQ to FMQ-2), though this is still the subject of debate (Lee *et al.*, 2005; Brandon & Draper, 1996; Carmichael, 1991). For reference, the expression describing the FMQ buffer is:

$$\log fO_2 = -26{,}494/T + 9.69 + 0.092(P-1)/T$$

where P = pressure in bars and T = temperature in Kelvin (Eugster & Wones, 1962).

Oxygen fugacity also controls the chemical reaction governing Fe partitioning between melt and $Au_{75}Pd_{25}$ capsules during rock-melting experiments:

$$FeO_{Melt} \leftrightarrow Fe_{Capsule} + \tfrac{1}{2}O_2$$

The equilibrium constant (K) for this reaction is defined as:

$$K = \frac{a_{Fe}^{Capsule}}{a_{FeO}^{Melt}} fO_2^{1/2} = \frac{\gamma_{Fe} X_{Fe}^{Capsule}}{\gamma_{FeO} X_{FeO}^{Melt}} fO_2^{1/2} = \frac{\gamma_{Fe}^{Capsule}}{\gamma_{FeO}^{Melt}} D_{Fe} fO_2^{1/2}$$

where a = activity, γ = activity coefficient, X = mole fraction, and D_{Fe} = Fe partition coefficient ($D_{Fe} = X_{Fe}^{Capsule}/X_{FeO}^{Melt}$). The standard state change in Gibbs free energy for the reaction is defined as:

$$\Delta G_r^\circ = -RT \ln K$$

where R = gas constant and T = temperature in Kelvin. Expanding ΔG_r°, substituting for K, and solving for ln D_{Fe} yields:

$$\ln D_{Fe} = -\tfrac{1}{2}\ln fO_2 - \ln \frac{\gamma_{Fe}^{Capsule}}{\gamma_{FeO}^{Melt}} - \frac{\Delta Hr^{o}}{RT} + \frac{\Delta Sr^{o}}{R} + \frac{\Delta Vr^{o}(P-1)}{RT}$$

where P = pressure in bars and T = temperature in Kelvin.

To create a simple predictive equation, I retain the thermodynamic form:

$$\ln D_{Fe} = a \ln fO_2 + b/T + c$$

Once calibrated, this relationship can be used to determine the prevailing oxygen fugacity of rock-melting experiments in (Fe)$Au_{75}Pd_{25}$ capsules, given the measured Fe-content of a capsule equilibrated with an experimental melt. This calibration will also predict the appropriate Fe-content of an (Fe)$Au_{75}Pd_{25}$ alloy to effectively buffer fO_2 in experiments of this type. This has been previously established for Fe in Pt capsules (Kessel *et al.*, 2001; Grove *et al.*, 1981). Also, Fe-presaturation of AuPd capsules has been shown to reduce Fe-loss from silicate melt to capsule in rock-melting experiments (Gaetani & Grove, 1998; Kägi *et al.*, 2005).

There is a clear linear relationship between ln D_{Fe} and ln fO_2 at both 1200°C and 1300°C (Figure 6). A best-fit regression of the data against fO_2 and T (°C) returns:

$$\ln D_{Fe} = -0.3635 \ln fO_2 - 14{,}966/T + 5.179 \qquad (1)$$

(°C; $R^2 = 0.97$)

I employ this calibration later in this chapter to evaluate the fO_2 that prevailed in my high-pressure experiments. I will also address the

fact that the expression given in (1) does not account for the pressure dependence of fO_2, as all experiments were run at 1 atm.

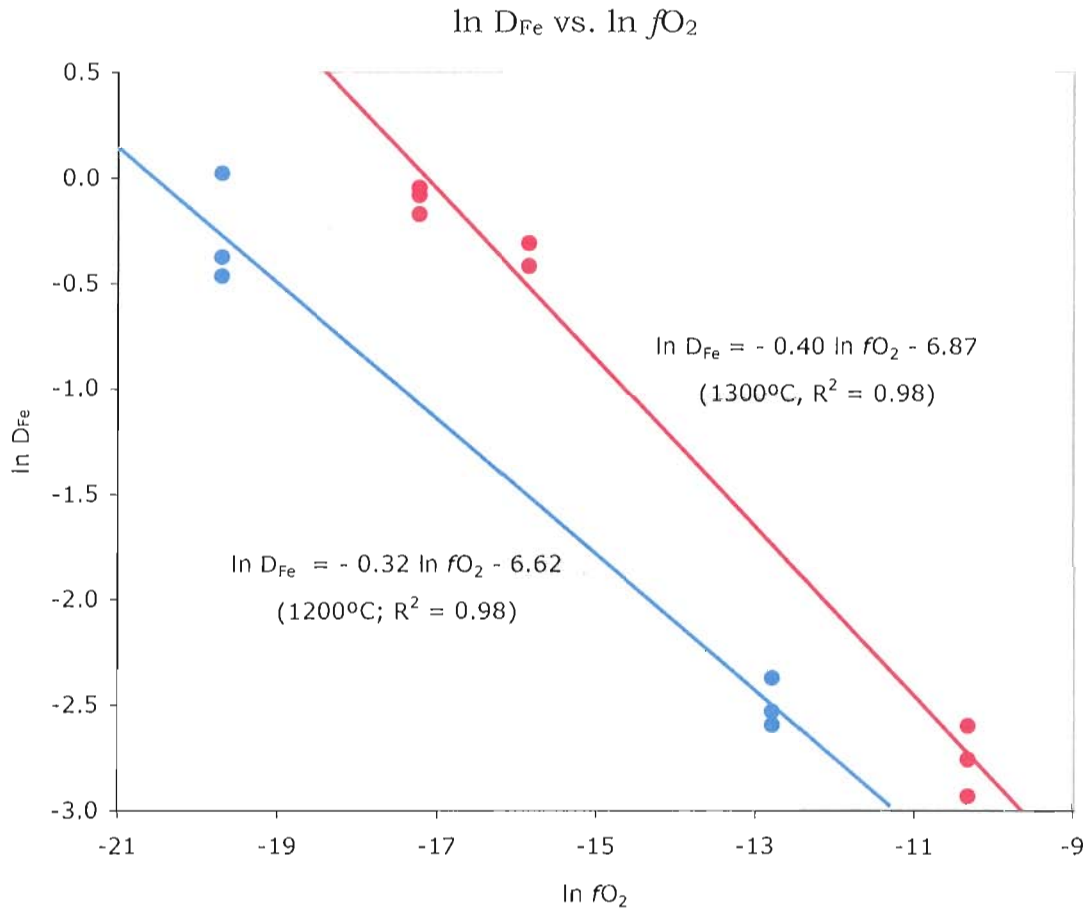

Figure 6. Variation in ln $X_{Fe}^{Capsule}/X_{FeO}^{Melt}$ partition coefficient with ln fO_2 at 1200 and 1300°C. Regressions for individual temperatures are shown. Regression against both fO_2 and T (°C) given in (1).

Near-Liquidus Phase Relations for the Pelagatos Composition

Near-liquidus experiments can constrain permissible mineral assemblages and compositions with which a melt could be in equilibrium over a range of P-T-X_{H2O} conditions. Since the melt fractions (F) approach 100%, the experimental melt compositions closely resemble the bulk sample composition. Therefore, identities and compositions of minerals present in the run products are interpreted as permissible phases or phase assemblages with which the bulk sample could have been in equilibrium at the P-T-X_{H2O} conditions of the experiments. The efficacy of this experimental approach improves as melt fractions approach 100%, with both the phase identity and compositions accurately representing a permissible residue in the limit of F = 0.999. In runs with greater crystallinities, but still only one crystalline phase, the phase identity would still be that of a permissible residue, but the composition will differ due to the compositional evolution of the coexisting equilibrium melt.

Calculated Phase Equilibria

To get an approximation of what the high-P experiments might reveal, I first performed numerical simulations of the P-T-X_{H2O} near-liquidus phase equilibria of the Pelagatos (d-25, Table 1) composition using the pMELTS software package (Ghiorso *et al.*, 2002). This model

utilizes a free energy minimization scheme and is optimized for elevated pressure calculations because it draws on a calibration database including results from high-pressure experiments. However, the database contains relatively few hydrous experimental results, so I place most confidence in the anhydrous results and view predictions under hydrous conditions as rough guides only. The hydrous experiments reported next provide a test of the accuracy of the pMELTS calculations.

Figure 7 shows the calculated phase relations using a range of water contents and the Pelagatos composition. P-T-X_{H2O} conditions within a single-phase field represent those under which the Pelagatos (d-25) bulk composition would be in equilibrium with just that phase. Conditions corresponding to the ol-opx, opx-cpx field boundaries represent P-T-X_{H2O} combinations under which the Pelagatos composition would be in equilibrium with harzburgite or pyroxenite respectively.

The Pelagatos magma contains a minimum of ~3 wt% H_2O, as shown by FTIR measurements of olivine-hosted melt inclusions (Roberge, unpublished data). The calculated pMELTS results suggest equilibration with a harzburgite assemblage at ~3 wt% H_2O, ~11 kbar, and ~1250°C. Higher water contents stabilize olivine to higher pressure and lower temperature. The calculated results also indicate that the Pelagatos composition may have been in equilibrium with a pyroxenite assemblage at ~3 wt% H_2O, ~13 kbar, and ~1260°C. Given the uncertainty involved

in the calculation, one could also interpret the near-intersection of all three (ol-opx-cpx) phase fields at ~3 wt% H_2O, ~1255°C, and ~12 kbar, to allow possible equilibration with a lherzolite assemblage.

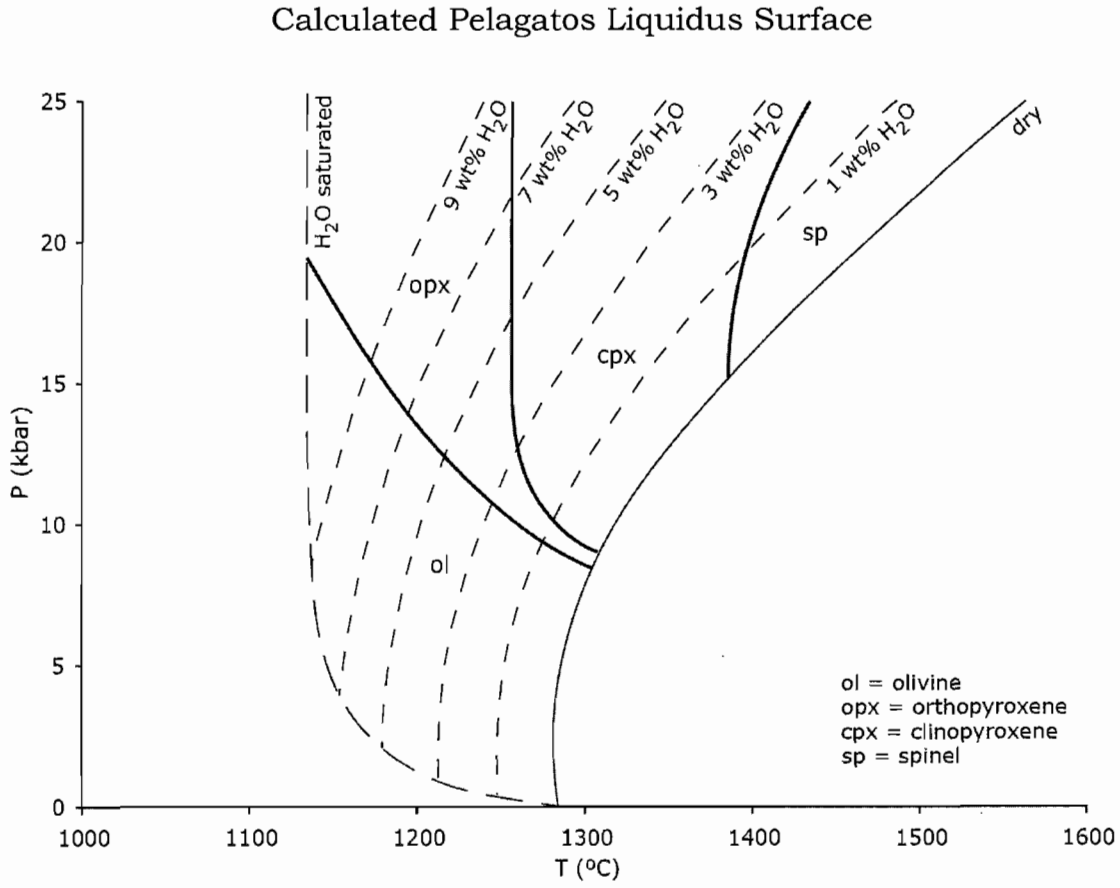

Figure 7. H_2O-undersaturated liquidus surface for the Pelagatos composition calculated using pMELTS (Ghiorso *et al.*, 2002).

Experimental Phase Equilibria

Electron microprobe analyses of all phases in all run products and capsule alloys are given in Tables 6 and 7, and a comparison of the glass analyses with the bulk composition in Table 1 provides a rough measure of the proximity of the run temperature to the samples liquidus at the pressure and H_2O content of the experiment. This can be evaluated more quantitatively from the run product modes in Table 5, which were calculated by least-squares mass balance using a spreadsheet kindly provided by Dr. David Draper. All runs except two (RW-3, F=0.8 and RW-8, F=0.8) had melt fractions (F) exceeding 0.93.

The near-liquidus RW runs (bold in Table 6) delineate the H_2O-undersaturated P-T liquidus surface for the Pelagatos composition, shown in Figure 8, and enable mapping of the liquidus surface mineralogy. Phase boundaries and P-T-X_{H2O} conditions are interpreted as previously described. Given the known crustal thickness (40-50 km) in this region, equilibration at pressures below 10.6 kbar can be ruled out, as this would be within the crust. Therefore, given the minimum water contents (~3 wt%), the Pelagatos magma could have equilibrated with a harzburgite residue at >7 wt% H_2O, 1080-1150°C, and 11-14 kbar or a pyroxenite residue at ~3 wt% H_2O, 1280-1350°C, and 14-20 kbar. I later explore the impact of adjusting the Pelagatos composition to be in

equilibrium with Fo_{92} olivine (to simulate a more refractory mantle source) on the interpretation of these results.

Table 5. Experimental Run Conditions and Assemblages

P (kbar)	Run	T (°C)	Dur. (h)	Glass[a]	Olivine	Opx	Cpx	Spinel	Σr^{2b}
~3 wt% H_2O									
7	RW-11	1200	18	99	1			trace	0.29
	RW-10	1225	18	100					
10	RW-9	1200	16.5	93	3	4			1.49
	RW-4	1220	16	100					
	RW-1	1240	16	100					
13	RW-8	1245	16.5	80		9	11		1.16
	RW-7	1265	18	95		5			0.35
15	RW-3	1285	17.5	80		9	11		0.11
	RW-6	1305	18	100					
20	RW-2	1345	16	94		5	1		0.33
~5 wt% H_2O									
10	RW-20	1165	16	93	2	5		trace	1.11
	RW-16	1185	12.5	100					
	RW-14	1205	16	100					
13	RW-17	1205	12.5	99		1			0.53
15	RW-19	1225	16.5	96		4			0.38
	RW-13	1245	16	100					
20	RW-25	1255	14	100					
	RW-18	1275	16.5	100					
	RW-12	1295	18	100					
~7 wt% H_2O									
12	RW-24	1140	14	97	2	1		trace	1.82
14	RW-22	1160	16	95		5			0.65

[a] Modes calculated by least-squares mass balance
[b] Σr^2 = sum of the squares of the residuals

Table 6. Electron Microprobe Analyses of High-P Run Products

P (kbar)	Run	T (°C)	Phase	SiO_2	TiO_2	Al_2O_3	Cr_2O_3	FeO_T[a]	NiO	MnO	MgO
~3 wt% H_2O											
7	**RW-11**	1200	Glass (*n*=4)	52.23(2)	0.81(1)	14.99(9)	0.06(2)	7.61(8)	*NA*	0.12(2)	9.07(3)
			Olivine (7)	40.00(39)	0.02(1)	0.04(1)	0.06(2)	11.01(42)	0.31(11)	0.14(2)	48.53(35)
	RW-10	1225	Glass (7)	52.81(37)	0.80(3)	15.13(17)	0.07(2)	7.56(9)	0.01(1)	0.13(1)	9.60(7)
10	**RW-9**	1200	Glass (7)	52.23(53)	0.87(5)	16.24(9)	0.04(2)	6.51(3)	*MDL*	0.14(1)	7.78(2)
			Olivine (7)	38.76(28)	0.02(2)	0.04(1)	0.03(2)	12.22(11)	0.10(1)	0.18(1)	47.51(12)
			Opx (7)	54.37(57)	0.15(2)	3.44(70)	0.67(17)	8.05(19)	*NA*	0.17(2)	30.83(39)
	RW-4	1220	Glass (4)	50.55(28)	0.77(3)	14.46(12)	0.07(2)	7.77(11)	*NA*	0.13(2)	9.42(12)
	RW-1	1240	Glass (5)	52.25(50)	0.79(3)	15.08(8)	0.08(2)	7.79(6)	*MDL*	0.12(2)	8.94(2)
13	RW-8	1245	Glass (3)	52.86(3)	0.87(2)	16.81(25)	0.04(2)	7.54(32)	*NA*	0.13(1)	7.51(5)
			Opx (3)	55.08(138)	0.14(3)	3.74(155)	0.50(6)	8.39(54)	*NA*	0.16(0)	31.17(81)
			Cpx (5)	53.53(35)	0.94(2)	18.00(44)	0.03(1)	7.50(63)	*NA*	0.12(1)	6.03(37)
	RW-7	1265	Glass (7)	51.95(19)	0.83(4)	15.74(18)	0.05(1)	7.47(13)	*NA*	0.13(1)	8.67(5)
			Opx (7)	54.55(47)	0.11(2)	4.10(24)	0.75(10)	7.65(19)	*NA*	0.15(1)	31.18(8)
15	**RW-3**	1285	Glass (5)	54.32(17)	0.97(2)	17.50(13)	0.03(1)	6.25(8)	*NA*	0.11(1)	6.18(23)
			Opx (4)	53.75(28)	0.23(7)	7.15(120)	0.27(4)	8.66(32)	*NA*	0.16(2)	27.15(201)
			Cpx (4)	51.44(63)	0.33(3)	7.44(110)	0.26(11)	7.92(28)	*NA*	0.20(2)	19.09(67)
	RW-6	1305	Glass (7)	52.07(37)	0.79(3)	15.17(8)	0.08(2)	7.95(7)	0.01(1)	0.11(2)	9.52(6)
20	**RW-2**	1345	Glass (7)	52.15(30)	0.87(2)	15.46(19)	0.04(1)	7.40(16)	*NA*	0.13(2)	8.25(5)
			Opx (7)	54.60(51)	0.09(2)	4.94(58)	0.54(8)	8.00(14)	*NA*	0.14(2)	29.92(21)
			Cpx (2)	49.27(194)	0.78(17)	14.22(330)	0.05(2)	8.36(26)	*NA*	0.18(3)	13.49(120)

Table 6. extended

P (kbar)	Run	T (°C)	Phase	CaO	Na_2O	K_2O	P_2O_5	H_2O^b	Total	Mg#[c]
~3 wt% H_2O										
7	**RW-11**	1200	Glass (*n*=4)	7.28(22)	3.49(11)	0.91(4)	0.15(2)	3.27(3)	100.00(0)	74.4
			Olivine (7)	0.15(3)	*MDL*	*MDL*	0.02(2)	0.00(0)	100.29(46)	91.5
	RW-10	1225	Glass (7)	7.34(9)	3.35(6)	0.91(1)	0.14(1)	2.15(42)	100.00(0)	75.6
10	**RW-9**	1200	Glass (7)	8.10(21)	3.84(27)	1.04(1)	0.15(1)	3.06(50)	100.00(0)	74.5
			Olivine (7)	0.19(2)	*MDL*	*MDL*	*MDL*	0.00(0)	99.06(26)	90.5
			Opx (7)	1.78(17)	0.07(2)	*MDL*	*MDL*	0.00(0)	99.52(37)	90.1
	RW-4	1220	Glass (4)	7.19(11)	4.72(11)	0.73(1)	0.14(2)	4.04(34)	100.00(0)	74.7
	RW-1	1240	Glass (5)	7.18(13)	3.27(29)	0.95(1)	0.13(1)	3.44(26)	100.00(0)	73.7
13	RW-8	1245	Glass (3)	7.71(12)	3.68(11)	1.03(0)	0.16(1)	1.65(5)	100.00(0)	70.8
			Opx (3)	1.62(22)	0.10(2)	0.01(0)	*MDL*	0.00(0)	100.88(12)	90.1
			Cpx (5)	7.99(26)	3.28(97)	0.82(2)	0.18(1)	0.00(0)	98.41(100)	66.3
	RW-7	1265	Glass (7)	7.35(18)	3.68(17)	0.94(2)	0.15(1)	3.03(19)	100.00(0)	73.9
			Opx (7)	1.50(15)	0.09(3)	*MDL*	*MDL*	0.00(0)	100.08(39)	90.9
15	**RW-3**	1285	Glass (5)	7.49(13)	3.96(15)	1.16(2)	0.18(1)	1.84(34)	100.00(0)	70.7
			Opx (4)	2.26(58)	0.37(21)	0.06(5)	0.01(1)	0.00(0)	100.09(14)	88.4
			Cpx (4)	12.09(60)	0.88(10)	0.01(1)	*MDL*	0.00(0)	99.67(42)	85.5
	RW-6	1305	Glass (7)	7.43(23)	3.31(8)	0.92(1)	0.13(1)	2.52(25)	100.00(0)	74.5
20	**RW-2**	1345	Glass (7)	7.77(15)	3.75(18)	0.98(1)	0.16(1)	3.04(28)	100.00(0)	73.1
			Opx (7)	1.65(12)	0.20(3)	0.00(0)	*MDL*	0.00(0)	100.06(28)	90.1
			Cpx (2)	12.06(160)	1.23(13)	0.06(4)	0.11(2)	0.00(0)	99.81(186)	79.8

Table 6. continued

P (kbar)	Run	T (°C)	Phase	SiO_2	TiO_2	Al_2O_3	Cr_2O_3	FeO_T[a]	NiO	MnO	MgO
~5 wt% H_2O											
10	**RW-20**	1165	Glass (5)	50.73(28)	0.82(3)	15.51(10)	0.05(1)	6.94(13)	*NA*	0.12(1)	7.64(2)
			Olivine (6)	38.83(17)	0.02(4)	0.06(9)	0.03(2)	12.38(31)	0.16(2)	0.14(4)	46.99(62)
			Opx (5)	57.09(23)	0.08(1)	1.47(3)	0.47(3)	8.06(11)	*NA*	0.17(2)	32.05(5)
	RW-16	1185	Glass (4)	50.87(30)	0.82(3)	14.62(9)	0.07(1)	7.42(3)	*NA*	0.13(2)	9.32(8)
	RW-14	1205	Glass	*NA*	*NA*	*NA*	*NA*	*NA*	*NA*	*NA*	*NA*
13	**RW-17**	1205	Glass (3)	50.89(8)	0.83(2)	14.88(13)	0.07(0)	7.21(26)	*NA*	0.13(1)	9.15(4)
			Opx (6)	54.79(27)	0.10(1)	3.62(31)	0.90(2)	7.57(17)	*NA*	0.16(1)	31.76(10)
15	**RW-19**	1225	Glass (4)	50.64(36)	0.80(6)	15.25(13)	0.05(1)	7.72(12)	*NA*	0.12(1)	8.36(3)
			Opx (7)	54.67(30)	0.11(1)	3.72(27)	0.68(11)	7.65(38)	*NA*	0.16(1)	31.42(14)
	RW-13	1245	Glass (4)	50.65(33)	0.78(1)	14.96(12)	0.08(2)	8.60(9)	*NA*	0.13(1)	9.08(2)
20	RW-25	1255	Glass (7)	52.01(36)	0.77(6)	14.66(10)	0.07(1)	7.75(4)	0.01(1)	0.13(2)	9.44(5)
	RW-18	1275	Glass (3)	50.31(24)	0.80(1)	14.70(2)	0.09(2)	7.77(5)	*NA*	0.11(3)	9.50(3)
	RW-12	1295	Glass	*NA*	*NA*	*NA*	*NA*	*NA*	*NA*	*NA*	*NA*
~7 wt% H_2O											
12	**RW-24**	1140	Glass (7)	51.80(20)	0.78(3)	14.95(21)	0.04(2)	7.26(5)	*MDL*	0.12(1)	8.09(5)
			Olivine (8)	39.79(49)	*MDL*	0.03(2)	0.04(3)	11.74(32)	0.30(4)	0.17(2)	47.82(36)
			Opx (6)	56.06(60)	0.10(3)	2.40(88)	0.86(22)	7.83(16)	0.07(1)	0.15(2)	32.15(54)
14	**RW-22**	1160	Glass (7)	49.86(19)	0.81(3)	15.08(13)	0.05(1)	7.53(9)	*NA*	0.14(1)	8.00(4)
			Opx (7)	54.79(23)	0.12(3)	3.94(46)	0.51(17)	7.72(27)	*NA*	0.16(1)	31.27(15)

Table 6. continued extended

P (kbar)	Run	T (°C)	Phase	CaO	Na_2O	K_2O	P_2O_5	H_2O^b	Total	Mg#[c]
~5 wt% H_2O										
10	**RW-20**	1165	Glass (5)	7.23(13)	5.02(11)	0.74(2)	0.14(1)	5.06(39)	100.00(0)	72.9
			Olivine (6)	0.14(4)	*MDL*	0.01(1)	*MDL*	0.00(0)	98.96(25)	90.3
			Opx (5)	1.42(9)	0.04(2)	*MDL*	*MDL*	0.00(0)	100.85(23)	90.7
	RW-16	1185	Glass (4)	7.05(11)	4.31(20)	0.76(3)	0.14(2)	4.48(36)	100.00(0)	75.4
	RW-14	1205	Glass	*NA*	*NA*	*NA*	*NA*	*NA*	*NA*	*NA*
13	**RW-17**	1205	Glass (3)	7.06(7)	4.49(6)	0.79(1)	0.14(0)	4.35(20)	100.00(0)	75.6
			Opx (6)	1.34(8)	0.06(3)	*MDL*	*MDL*	0.00(0)	100.30(59)	91.1
15	**RW-19**	1225	Glass (4)	7.11(12)	4.55(29)	0.82(2)	0.14(1)	4.43(19)	100.00(0)	72.6
			Opx (7)	1.36(7)	0.09(3)	0.01(0)	*MDL*	0.00(0)	99.84(30)	90.9
	RW-13	1245	Glass (4)	6.90(36)	3.36(34)	0.86(3)	0.14(1)	4.46(31)	100.00(0)	72.1
20	RW-25	1255	Glass (7)	7.36(19)	3.44(14)	0.89(1)	0.13(1)	3.33(23)	100.00(0)	74.8
	RW-18	1275	Glass (3)	7.01(0)	4.45(9)	0.79(1)	0.15(0)	4.33(18)	100.00(0)	74.9
	RW-12	1295	Glass	*NA*	*NA*	*NA*	*NA*	*NA*	*NA*	*NA*
~7 wt% H_2O										
12	**RW-24**	1140	Glass (7)	7.13(17)	2.21(56)	0.87(1)	0.13(1)	6.61(52)	100.00(0)	73.1
			Olivine (8)	0.14(2)	*MDL*	*MDL*	*MDL*	0.00(0)	100.24(29)	90.9
			Opx (6)	1.32(11)	0.04(1)	*MDL*	*MDL*	0.00(0)	100.96(28)	90.9
14	**RW-22**	1160	Glass (7)	7.19(17)	3.24(17)	0.87(3)	0.15(2)	7.07(46)	100.00(0)	72.2
			Opx (7)	1.42(20)	0.06(2)	*MDL*	*MDL*	0.00(0)	99.98(20)	90.8

Microprobe analyses in wt%; run labels in bold print denote experiments used to construct the phase diagram in Figure 8; numbers in parentheses next to each analysis represent 1σ standard deviation on average of multiple analyses; errors given in terms of least unit cited [e.g., 52.23(2) represents 52.23 ± 0.02]

n number of analyses, *NA* not analyzed, *MDL* below minimum 99% detection limit

[a] All Fe reported as FeO_T

[b] H_2O calculated iteratively by difference, adjusting ZAF corrections with each iteration

[c] Mg# = 100 x molar[MgO/(MgO+FeO)]; FeO/FeO_T=0.73 (Kress & Carmichael, 1991)

Table 7. Electron Microprobe Analyses of High-P Capsule Alloys

Run	Fe wt%	Au wt%	Pd wt%	Mn wt%	Ni wt%	Total
RW-1 (*n*=5)	0.60(1)	73.08(48)	26.91(28)	*MDL*	0.04(1)	100.62(27)
RW-2 (5)	0.56(3)	72.97(34)	27.13(22)	*MDL*	0.01(1)	100.68(34)
RW-3 (5)	1.12(3)	71.86(33)	25.20(23)	*NA*	*NA*	98.19(38)
RW-4 (5)	0.48(2)	73.51(42)	26.80(20)	*MDL*	0.01(1)	100.80(40)
RW-6 (5)	0.53(1)	72.82(58)	25.50(26)	*NA*	*NA*	98.84(85)
RW-7 (5)	0.41(1)	73.13(19)	26.82(16)	*NA*	*NA*	100.36(9)
RW-8 (5)	0.40(2)	73.74(22)	26.70(15)	*NA*	*NA*	100.84(36)
RW-9 (5)	0.82(2)	71.97(14)	25.69(12)	*NA*	*NA*	98.48(17)
RW-10 (5)	0.56(0)	72.16(19)	25.56(4)	*NA*	*NA*	98.28(16)
RW-11 (5)	0.49(1)	73.43(30)	26.77(33)	*NA*	*NA*	100.69(32)
RW-13 (5)	0.32(2)	73.11(36)	25.11(14)	*NA*	*NA*	98.53(30)
RW-16 (5)	0.47(1)	72.51(12)	25.63(7)	*NA*	*NA*	98.62(10)
RW-17 (5)	0.39(2)	72.71(23)	26.95(15)	*NA*	*NA*	100.05(15)
RW-18 (5)	0.42(1)	73.13(32)	25.48(22)	*NA*	*NA*	99.03(20)
RW-19 (5)	0.30(1)	72.77(52)	26.44(16)	*NA*	*NA*	99.51(57)
RW-20 (5)	0.37(2)	72.53(24)	25.45(14)	*NA*	*NA*	98.34(35)
RW-22 (5)	0.35(1)	72.55(16)	25.71(10)	*NA*	*NA*	98.62(20)
RW-24 (5)	0.26(1)	73.64(21)	25.47(18)	*NA*	*NA*	99.37(17)
RW-25 (5)	0.38(1)	73.03(12)	25.62(3)	*NA*	*NA*	99.03(14)

Numbers in parentheses next to each analysis represent 1σ standard deviation on average of multiple analyses; errors given in terms of least unit cited [e.g., 0.60(1) represents 0.60 ± 0.01]

n number of analyses, *NA* not analyzed, *MDL* below minimum 99% detection limit

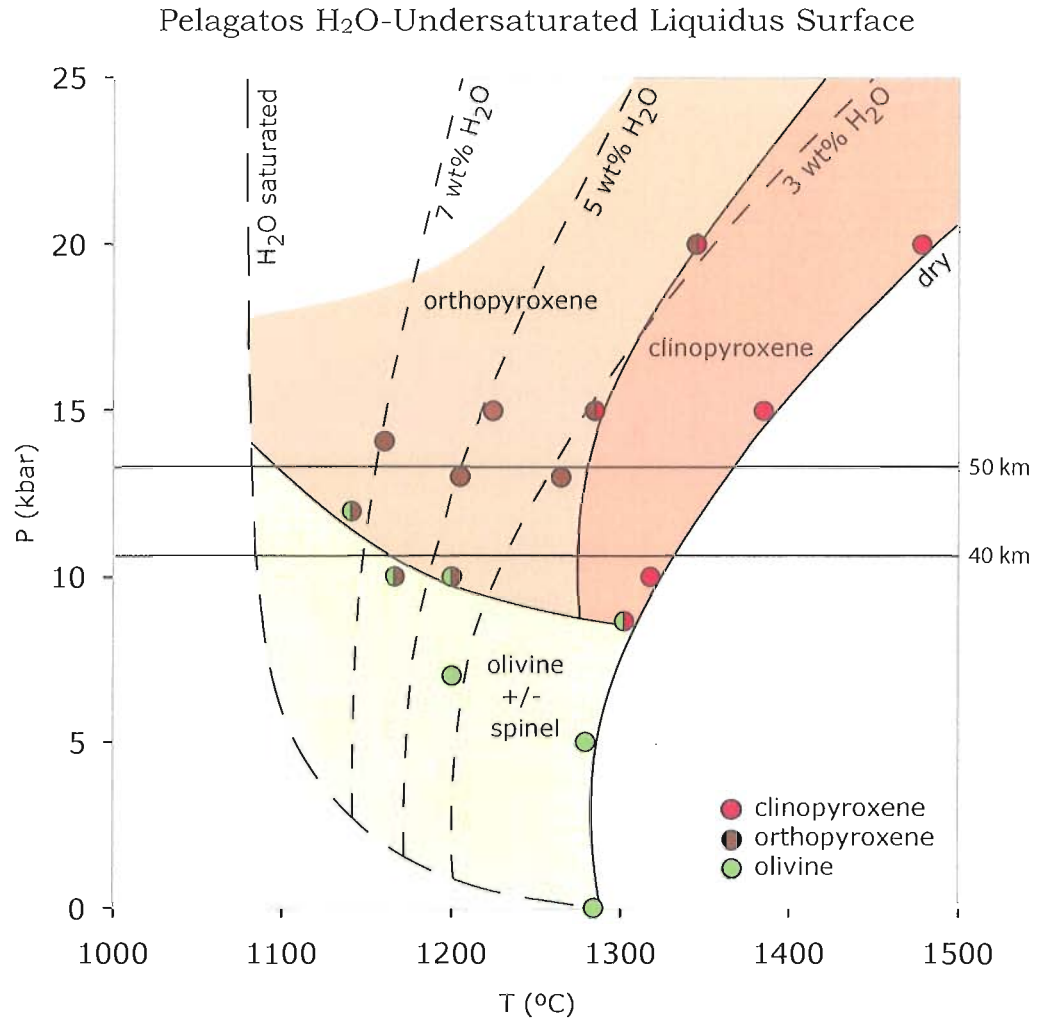

Figure 8. Water-undersaturated liquidus surface for the Pelagatos (d-25) composition. Dashed lines are isopleths of constant water contents. Data plotted along the dry liquidus represent calculated liquidus phases determined using pMELTS (Ghiorso *et al.*, 2002). Data along the 3, 5, and 7 wt% H_2O isopleths represent the ten near-liquidus experiments (analyses in Table 6). Sub-liquidus phase relations are not shown. Horizontal lines at 40 and 50 km represent a depth range for the base of the crust beneath the Pelagatos cinder cone.

The experimental results differ from results calculated with pMELTS in several important ways. In the experimental phase diagram, the water isopleths are steeper at higher H_2O contents, and the opx field is greatly expanded. The experimentally determined pyroxenite phase boundary approximately follows the 3 wt% H_2O curve and increases in temperature as pressure increases, while in the pMELTS calculations, the temperature of this boundary stays approximately constant as pressure increases. Also, in my high-P experiments, spinel was found only coexisting with olivine at lower pressures (<12 kbar), and the liquidus is generally shifted 20-40°C down temperature from the liquidus temperature predicted by pMELTS.

Trends in Mineral Compositions

It is difficult to define trends in mineral compositions with such a limited data set and with all runs at near-liquidus conditions. However, it is clear that Al_2O_3 content increases in orthopyroxene with pressure. This is the only observable trend in mineral compositions. There are noticeable differences in the minerals produced in runs RW-3 and RW-8, both of which are approximately 20% crystalline. Compared to my other high-P runs, orthopyroxene in RW-3 is Al-rich (7.15 vs. 1.5-5 wt%) and Mg-poor (27.15 vs. 29-32 wt%), while clinopyroxene is Al-poor (7.44 vs. 14-18 wt%) and Mg-rich (19.09 vs. 6-13.5 wt%). In sample RW-8,

orthopyroxene is similar in composition to the other RW samples, but clinopyroxene is Al-rich (18 vs. 7.5-14 wt%) and Ca- and Mg-poor (7.99 vs. 12 wt% and 6.03 vs. 13.5-19 wt%, respectively).

Oxygen Fugacity of High-P Experiments

Using the previously described calibration (Equation 1), the prevailing oxygen fugacity of rock-melting experiments in which basaltic to basaltic andesite melts are in equilibrium with (Fe)$Au_{75}Pd_{25}$ alloy at high temperature can be estimated from:

$$\log fO_2 = -2.751 \log D_{Fe} - 17880/T + 6.187 \quad (2)$$

(°C; $R^2 = 0.97$)

This relationship was used to estimate the fO_2 that prevailed in each of the high-P experiments. First, the glass FeO wt% and alloy Fe wt% values (EPMA data given in Tables 6 and 7) were converted to mole fractions and used to compute D_{Fe} (Table 8). Then, knowing the temperature of each experiment, experimental fO_2 values were computed from (2). These values are plotted against the experimental temperatures in Figure 9, where curves for the NNO buffer ($NiO = Ni + \frac{1}{2}O_2$; Huebner & Sato, 1970) and NNO+1 are shown. Also plotted are seven results on a different composition (S. Weaver, unpublished data) that utilized the same experimental procedures. These data illustrate the general applicability of the technique. From this plot, it appears that the

Table 8. Calculated fO_2 of High-P Experiments

Run	T (°C)	$X_{Fe}^{Capsule}$	X_{FeO}^{Melt}	D_{Fe}	log D_{Fe}	log fO_2[a]	fO_2[b]
d-25 starting material							
RW-1	1240	0.0169(4)	0.0699(5)	0.242(5)	-0.62	-6.54	NNO+0.7
RW-2	1345	0.0159(8)	0.0664(14)	0.239(14)	-0.62	-5.40	NNO+0.7
RW-3	1285	0.0322(9)	0.0565(8)	0.571(18)	-0.24	-7.06	NNO-0.4
RW-4	1220	0.0137(1)	0.0698(10)	0.196(3)	-0.71	-6.52	NNO+0.8
RW-6	1305	0.0153(4)	0.0705(6)	0.217(6)	-0.66	-5.69	NNO+0.7
RW-7	1265	0.0117(2)	0.0670(12)	0.175(5)	-0.76	-5.86	NNO+1
RW-8	1245	0.0113(6)	0.0674(29)	0.168(12)	-0.77	-6.04	NNO+1
RW-9	1200	0.0238(5)	0.0587(3)	0.405(8)	-0.39	-7.63	NNO
RW-10	1225	0.0163(1)	0.0666(5)	0.245(2)	-0.61	-6.73	NNO+0.6
RW-11	1200	0.0138(2)	0.0681(7)	0.203(4)	-0.69	-6.81	NNO+0.7
RW-13	1245	0.0092(5)	0.0780(8)	0.118(6)	-0.93	-5.62	NNO+1.4
RW-16	1185	0.0136(2)	0.0670(3)	0.204(3)	-0.69	-7.00	NNO+0.7
RW-17	1205	0.0111(5)	0.0652(24)	0.171(10)	-0.77	-6.54	NNO+0.9
RW-18	1275	0.0121(2)	0.0700(4)	0.173(3)	-0.76	-5.74	NNO+1
RW-19	1225	0.0086(4)	0.0703(11)	0.122(6)	-0.91	-5.90	NNO+1.4
RW-20	1165	0.0108(7)	0.0638(12)	0.169(11)	-0.77	-7.04	NNO+0.9
RW-22	1160	0.0103(3)	0.0706(8)	0.146(4)	-0.84	-6.93	NNO+1.1
RW-24	1140	0.0074(4)	0.0676(5)	0.109(6)	-0.96	-5.42	NNO+1.5
RW-25	1255	0.0109(3)	0.0692(4)	0.157(5)	-0.80	-7.29	NNO+1
JR-28 starting material (S. Weaver, unpublished data)							
CAB-2	1175	0.0161(22)	0.0608(12)	0.265(37)	-0.58	-7.47	NNO+0.4
CAB-3	1150	0.0100(16)	0.0545(11)	0.183(29)	-0.74	-7.36	NNO+0.8
CAB-4	1200	0.0174(14)	0.0582(6)	0.299(24)	-0.52	-7.29	NNO+0.3
CAB-5	1225	0.0185(6)	0.0649(6)	0.284(10)	-0.55	-6.92	NNO+0.4
CAB-7	1200	0.0190(7)	0.0644(8)	0.295(12)	-0.53	-7.27	NNO+0.3
CAB-8	1275	0.0201(6)	0.0625(11)	0.322(11)	-0.49	-6.49	NNO+0.3
CAB-9	1225	0.0212(8)	0.0614(8)	0.345(13)	-0.46	-7.15	NNO+0.2

Numbers in parentheses next to each analysis represent 1σ standard deviation; errors given in terms of least unit cited [e.g., 0.0169(4) represents 0.0169 ± 0.0004]

[a] Calculated using equation (2)

[b] Determined using NNO reference curves (Huebner & Sato, 1970)

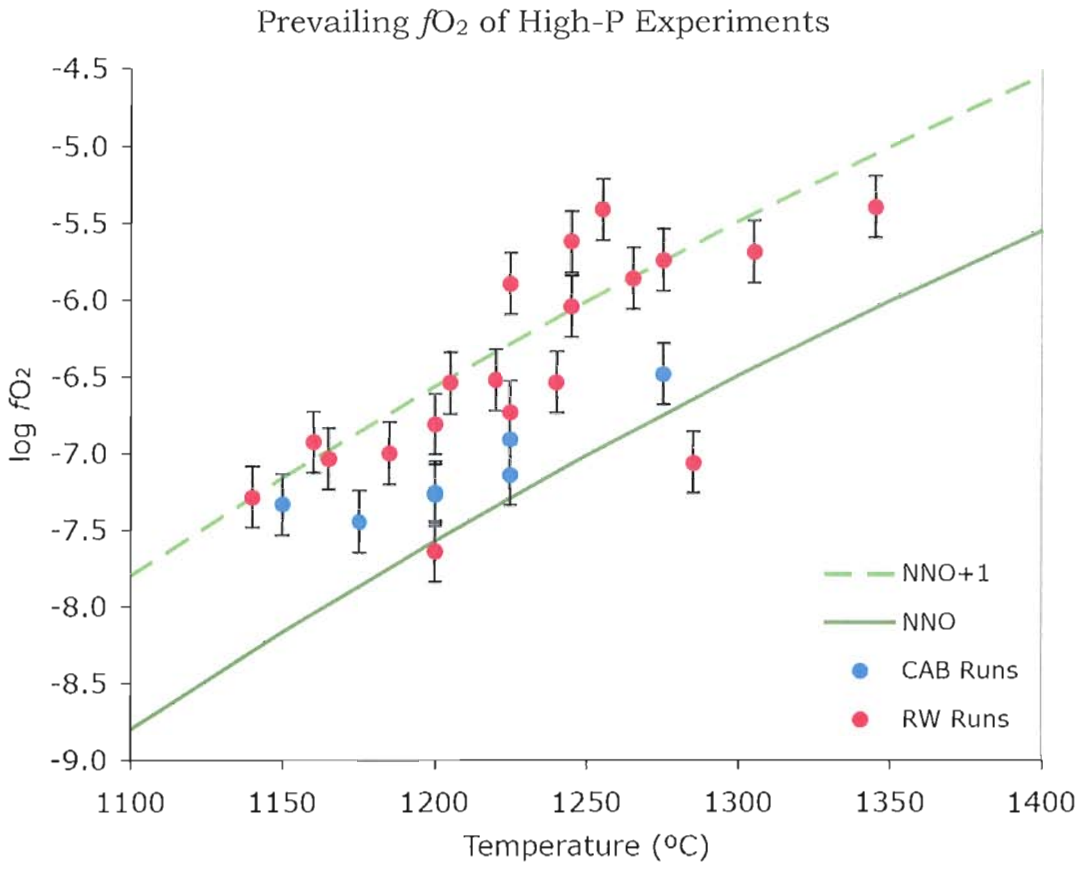

Figure 9. Piston-cylinder experiments for which I have applied this calibration. RW experiments are shown in red; CAB experiments (S. Weaver, unpublished data) are shown in blue. Error bars represent 2σ. NNO reference curves are from Huebner & Sato (1970). Virtually all high-P runs lie between NNO and NNO+1, indicating that the Au-Pd-Fe capsule material maintains fO_2 at the desired value.

Fe-presaturating procedures effectively controlled the experimental oxygen fugacities in the desired range.

As stated earlier, this calibration does not account for the pressure dependence of fO_2. The expression for the nickel-nickel oxide (NNO) buffer is:

$$\log fO_2 = -24{,}930/T + 9.36 + 0.046(P-1)/T$$

where P = pressure in bars and T = temperature in Kelvin (Haggerty, 1976; Huebner & Sato, 1970; Eugster & Wones, 1962). In this expression, 0.046 represents the change in molar volume of the solids. For example, at 10 kbar and 1300°C, the pressure difference from one bar would predict an fO_2 just 0.3 log units more oxidizing, which I consider to be within the uncertainties.

Water and Iron Loss

H_2O contents in near- and super-liquidus glasses were measured using the water-by-difference method in the Probe for EPMA software, calibrated by Roman *et al.*, (2006). Measured water contents are within ~1.5 wt% (absolute) of the nominal water contents (Figure 10), and in all near-liquidus experiments, they are within 1 wt% (absolute). Therefore, in all my hydrous high-pressure experiments, it appears that bulk water contents have been acceptably maintained.

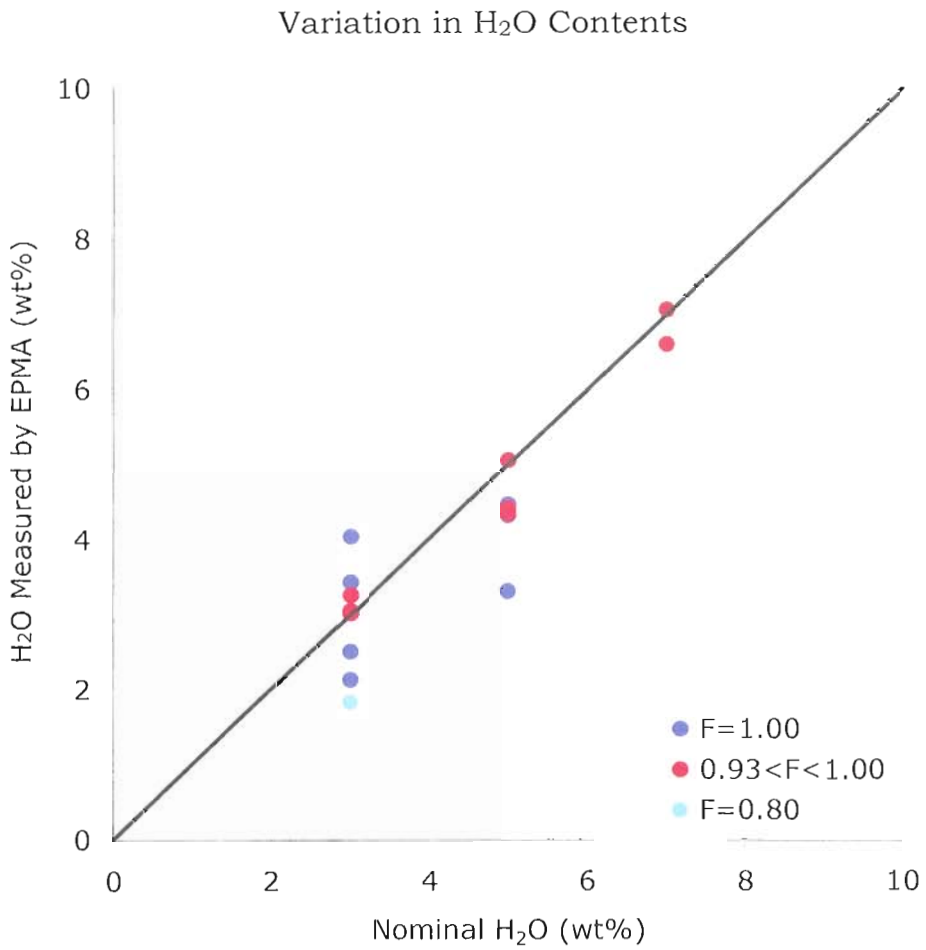

Figure 10. Variation in H_2O contents of near- and super-liquidus runs.

I observe iron gain from the presaturated (Fe)AuPd capsule to the melt in most of my high-P experiments with no apparent correlation between the relative amount of iron gained and water content. Fe-gain in the super-liquidus runs is most dramatic (generally 5-11 relative % and as high as 22 relative %). However, most near- and sub-liquidus runs gained <10 relative % Fe, and two near-liquidus melts appear to have lost

6-9 relative % Fe to the capsules. These results are shown in Figure 11. As noted earlier, Fe-gain in the melt from the (Fe)AuPd capsules indicates that shifting the fO_2 one long unit more reducing than the intrinsic fO_2 during presaturation (Médard *et al.*, 2008) dissolved slightly too much Fe into the capsule to be in equilibrium with the Pelagatos starting composition when re-used in a subsequent high-pressure experiment.

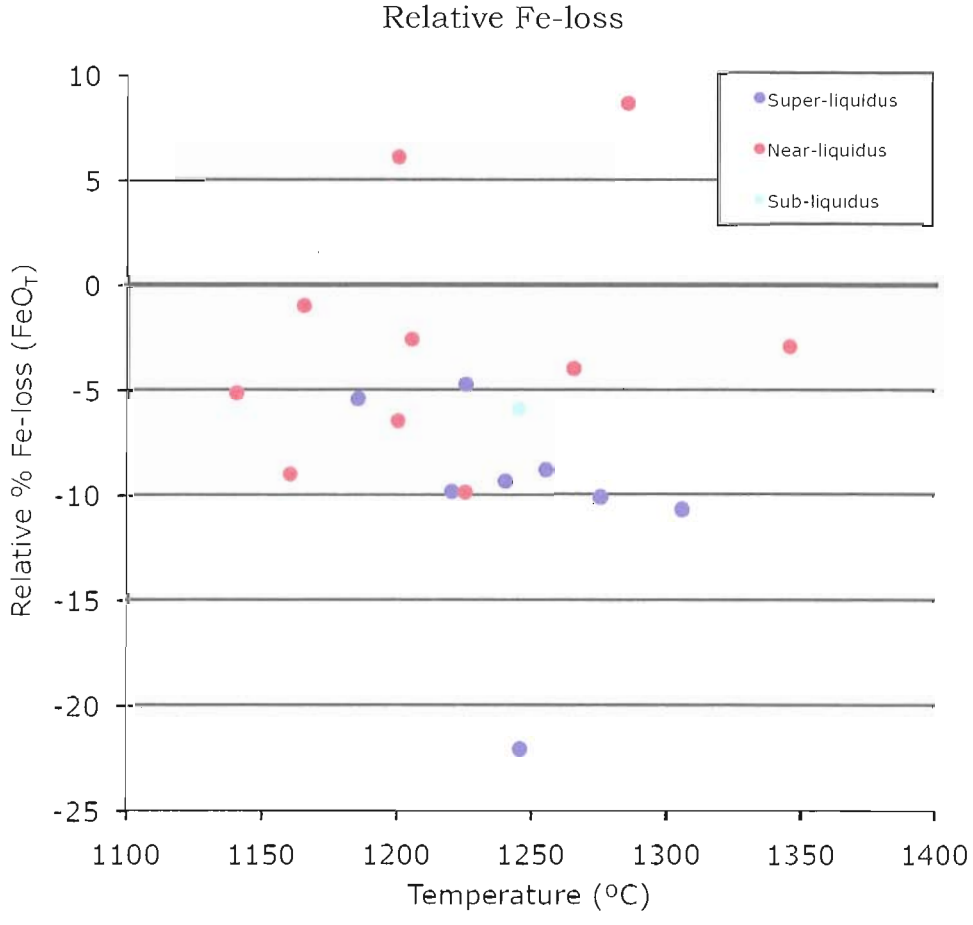

Figure 11. Relative Fe-loss in high-P piston-cylinder experiments.

CHAPTER IV

DISCUSSION

Permissible Residual Mantle Mineral Assemblages

Based on the experimentally determined phase diagram (Figure 8), the primitive Pelagatos magma could have equilibrated with either a harzburgite or pyroxenite residue within the mantle wedge. Straub *et al.* (2008) suggests a pyroxenite residue for higher SiO_2, lower MgO andesites from nearby Popocatépetl volcano based on analyses of Ni contents in olivine phenocrysts. The Straub *et al.* model utilizes serial melting, in which increasingly depleted mantle is repeatedly melted as it is fluxed by fluids from the slab. At low melt MgO contents, the very high olivine/melt D_{Ni} values promote the early crystallization of Ni-rich olivine (~5000-7200 ppm Ni in olivine) in melts produced by the partial melting of pyroxenite. In contrast, phenocrysts in more magnesian melts produced by the partial melting of peridotite contain only ~2500-3780 ppm Ni in olivine (Straub *et al.*, 2008).

Olivine phenocrysts in the Pelagatos (d-25) lava contain ~1300-3300 ppm Ni (Meriggi *et al.*, 2008), and olivine phenocrysts in my

experimental RW run products contain 1200-2400 ppm Ni (Figure 12). These results suggest that the Pelagatos composition was likely produced by the partial melting of a peridotite source, rather than a pyroxenite source. The calculated olivine fractionation paths in Figure 12 also suggest the possibility that the Pelagatos magma formed by melting of harzburgite and was subsequently affected by olivine crystallization after it segregated from the mantle source. This is discussed in more detail below in the following section.

Proposed Equilibration Conditions

Assuming that the Pelagatos composition was last in equilibrium with harzburgite (as supported by Figure 12), the experimental results can be compared with several published barometers for mantle melting to see if they are in agreement. I calculated the pressures of equilibrium with a harzburgite residue for different melt H_2O contents using the method developed by Wood & Turner (2009). This experimentally calibrated method combines the effects of both H_2O and clinopyroxene under-saturation on equilibrium pressures. At 3 wt% H_2O, pressure constraints from the experiments are in fairly good agreement with their model predictions. However, at higher water contents (>5 wt%), the model overestimates the pressures of equilibration by as much as 1 GPa at 7 wt% H_2O (Figure 13). My experimental results are in better

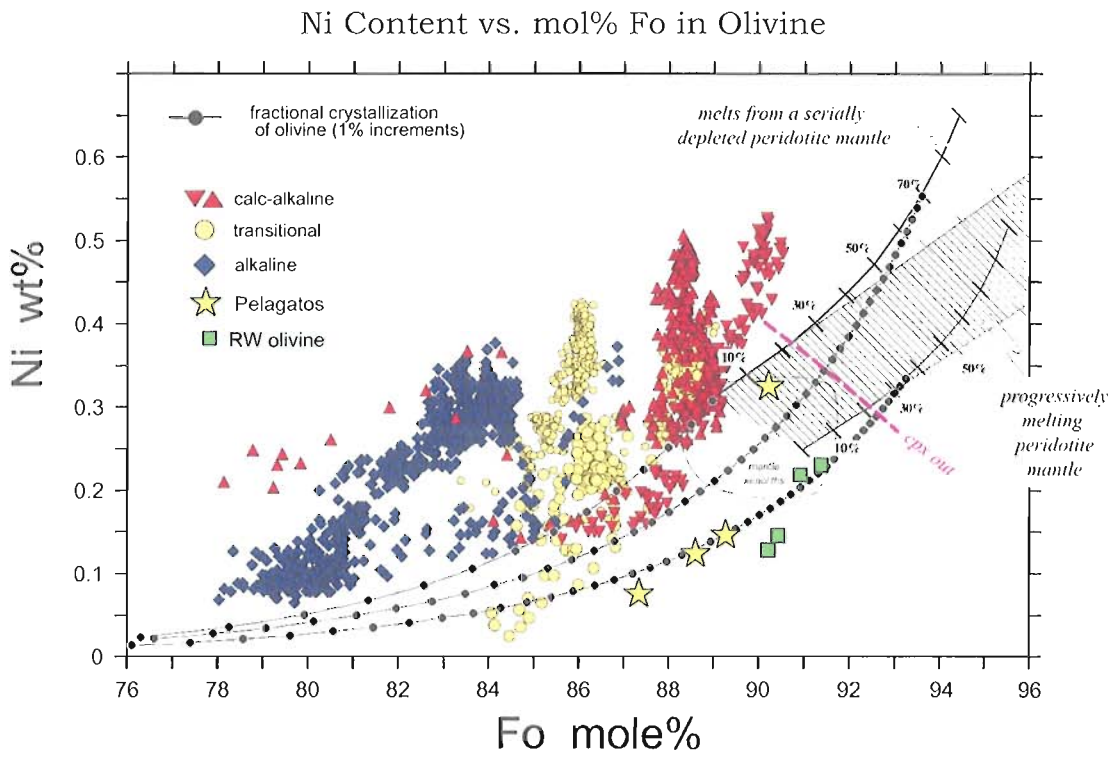

Figure 12. Ni content versus mole percent Fo for central TMVB olivine compared to the range of partial melts from peridotite. Mantle compositions are based on xenolith data representative of the upper mantle beneath the North American plate. Green field shows range of melts created from serially melted and depleted peridotite. Hatched field indicates range of melts generated by variable extent of melting (0-70%) from a single source. Lilac line indicates approximate point where clinopyroxene is exhausted from the residue (Straub *et al.*, 2008). Pelagatos olivines (yellow stars) fall in and below the region of a progressively melted peridotite. Experimental olivines (green squares) also fall below this region. Figure is modified from Straub *et al.* (2008).

Calculated Pressures for Equilibration with Harzburgite

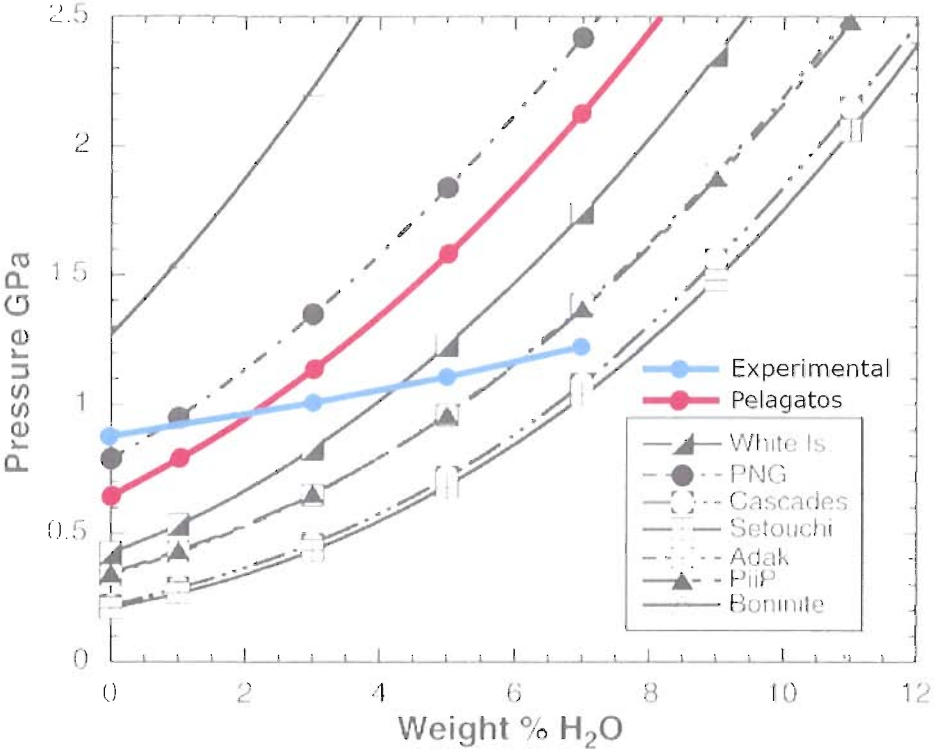

Figure 13. Curves describing the conditions of pressure and H_2O content under which melts could coexist with harzburgite residue (modified from Wood & Turner, 2009). The Pelagatos composition is represented by the red curve. White Is. = White Island, New Zealand; PNG = Amphlett Island, Papua New Guinea; Cascades = Mount Shasta, California; Setouchi = Setouchi Belt, Japan; Adak = Adak Island; PiiP = Piip volcano; Boninite is from Tonga. A comparison of this figure to the experimental ol-opx phase boundary (blue) shows the difference between the pressures of equilibration predicted by the Wood & Turner (2009) model and the pressures of equilibration indicated by the experimental data.

agreement with another published thermobarometer (Lee *et al.*, 2009) that is applicable to compositions in equilibrium with both olivine and orthopyroxene. Calculated results for my experimental glass composition (RW) containing 0, 3, 5, and 7 wt% H_2O are plotted on top of the experimental phase diagram in Figure 14. These results lie within error of the experimental line representing harzburgite equilibration.

The Lee *et al.* (2009) thermobarometer is based on SiO_2 activity, and it is calibrated using a large experimental database. To use the thermobarometer, magma compositions are first expressed in terms of mol% of molecular species, and silica activity is approximated by accounting for chemical interactions between oxides. The form of the calculation expresses pressure as a function of molar Si_4O_8 and temperature, including molar volume and entropy changes (Lee *et al.*, 2009). The agreement between the Lee et al. barometer and my experimental results suggests that the barometer is well calibrated for magma compositions from the Chichinautzin region.

My experimental results (RW runs) indicate equilibration with a harzburgite source only at high H_2O contents (>7 wt%) and relatively low temperatures (1100-1150°C) and pressures (11-14 kbar). However, the olivine fractionation paths from Straub *et al.* (2008) in Figure 12 suggest the possibility that the Pelagatos sample may represent the product of olivine fractionation from a magma that was derived from a more

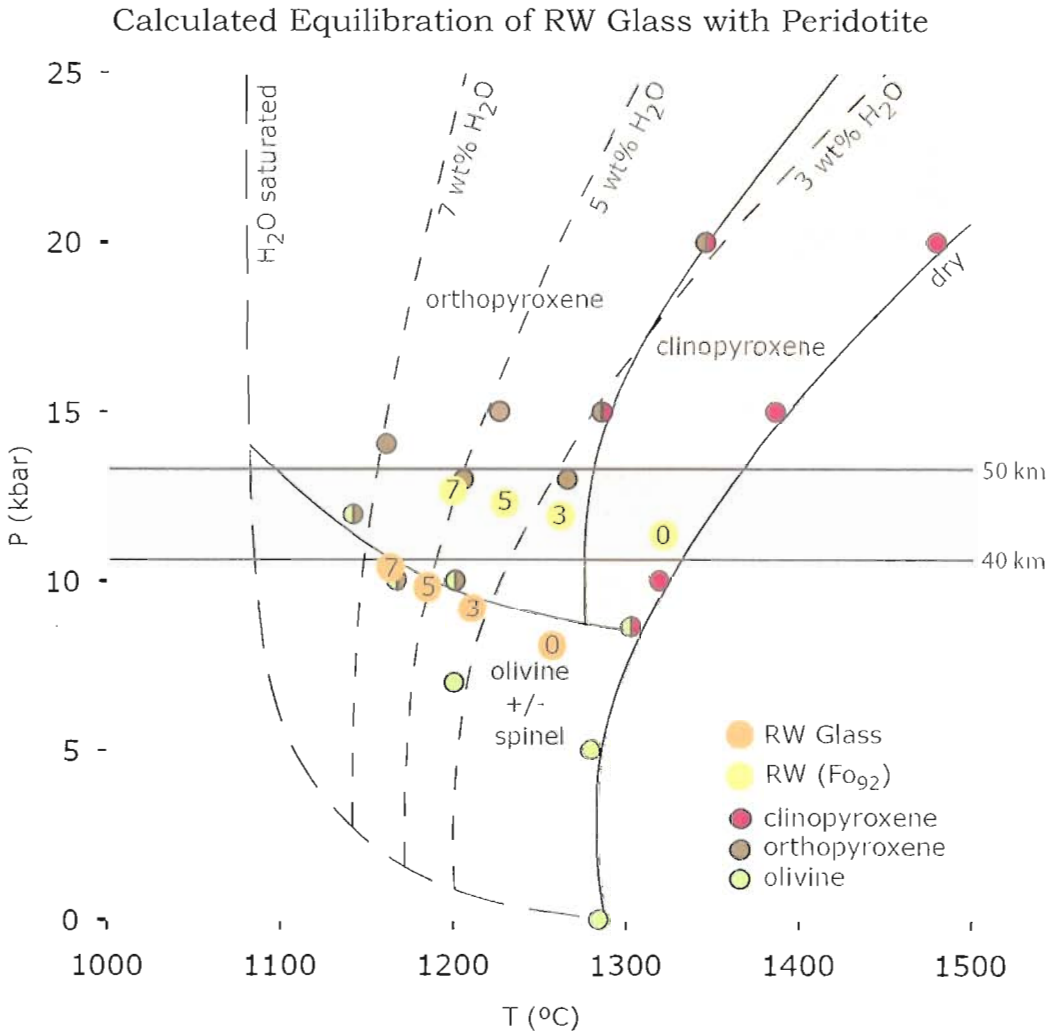

Figure 14. Water-undersaturated liquidus surface for the Pelagatos composition (see Figure 8 for full description) showing calculated equilibrium pressures and temperatures from Lee *et al.* (2009) for the RW ($Fo_{90.4}$) glass composition (orange) and adjusted RW (Fo_{92}) composition (yellow). Points represent 0, 3, 5, and 7 wt% H_2O (from right to left). As shown, the Lee *et al.* (2009) model is in good agreement with the ol-opx phase boundary for my experimental glasses (RW runs).

refractory source. To account for the possibility that such fractionation may have occurred during ascent, I numerically added 0.1 wt% increments of equilibrium olivine to the composition to force equilibrium with Fo_{92} olivine (e.g. Stolper & Newman, 1994). A total of 6.6 wt% olivine addition was required to achieve this equilibrium. My goal in doing this was to see if a more primitive composition would yield higher equilibrium pressure and temperature estimates by the method of Lee *et al.* (2009). I consider Fo_{92} to be an upper limit in terms of Fo content because the most Mg-rich olivines found in Chichinautzin lavas are $Fo_{91.4}$-$Fo_{91.8}$ (Wallace & Carmichael, 1999). This composition adjustment increases the pressure and temperature of equilibration with harzburgite, calculated using Lee *et al.* (2009), to just below the crust-mantle boundary (~13 kbar), close to the hottest part of the mantle wedge (Manea *et al.*, 2005).

In an effort to compare my results with other high-Mg andesites from the central TMVB, I used analyses of compositions with >8 wt% MgO from the CVF (Meriggi *et al.*, 2008; Wallace & Carmichael, 1999) and numerically added 0.1 wt% increments of equilibrium olivine until they were in equilibrium with Fo_{92} (e.g. Stolper & Newman, 1994). Totals of 5-14 wt% olivine were required to reach this equilibrium. I then applied the Lee *et al.*, (2009) thermobarometer to infer pressures and

temperatures at which these magmas could have equilibrated with harzburgite.

Figure 15 shows these results, along with the calculated pressures and temperatures in the mantle wedge based on the geodynamic model of Manea *et al.*, (2005). The peak mantle wedge temperature is ~1270°C and occurs at ~14 kbar. Magmas formed deeper than this would likely have re-equilibrated as they passed through the hottest part of the mantle during ascent. Since the base of the crust is at a minimum depth of 40 km (~10.6 kbar), the pressure of equilibration for the magmas from the Chichinautzin region can be constrained to 11-14 kbar.

The temperature of equilibration is more difficult to constrain because the liquidus temperatures of mantle melts are highly dependent on water content. If the peak mantle wedge temperature is ~1270°C at ~14 kbar, as determined by the Manea *et al.* (2005) model, the majority of Chichinautzin high-Mg lavas could have equilibrated with harzburgite, if the magmas contained 3-5 wt % H_2O at 1230-1270°C. The exceptions are the three compositions of this group with the highest SiO_2 contents, which appear to require 5-7 wt% H_2O at 1190-1200°C. Melt inclusion data for high-Mg basaltic andesites from the CVF contain 3-5 wt% H_2O (Cervantes & Wallace, 2003), consistent with harzburgite equilibration temperatures of 1230-1270°C.

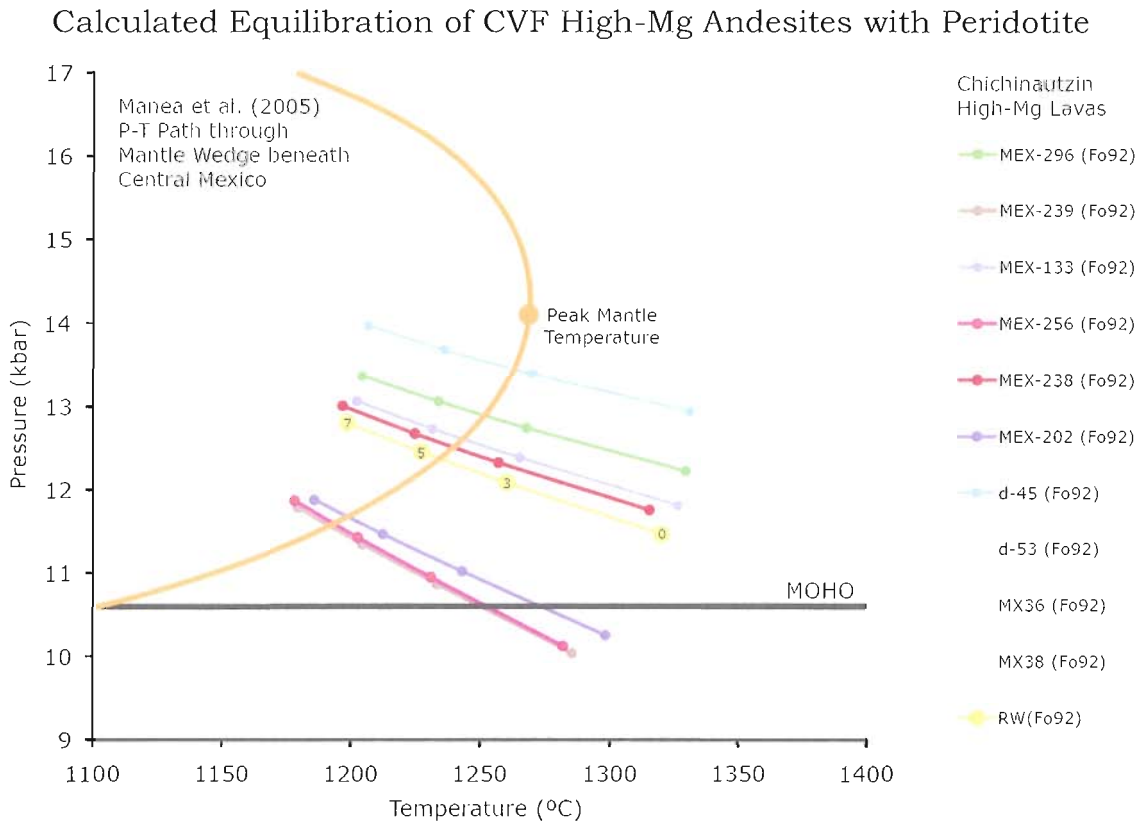

Figure 15. Calculated pressures and temperatures (Lee *et al.*, 2009) for high-Mg (>8 wt%) compositions from the CVF (Wallace & Carmichael, 1999; Meriggi *et al.*, 2008) numerically adjusted to equilibrium with Fo_{92} olivine. Points on each line represent 0, 3, 5, and 7 wt % H_2O (from right to left). Black horizontal line denotes the minimum depth of the MOHO (40 km). Orange curved line denotes the P-T path through the inverted thermal gradient of the mantle wedge beneath the central TMVB, as modeled by Manea *et al.* (2005). Yellow line represents the composition of the RW glass numerically adjusted to equilibrium with Fo_{92} olivine.

CHAPTER V

SUMMARY AND CONCLUSION

The hydrous, high-pressure experiments described here provide compositional and P-T-X_{H2O} constraints on permissible mantle mineral assemblages which the Pelagatos magma last equilibrated with prior to eruption. Combining my experimental results with the known crustal thickness of the region, a published thermobarometer, and a geophysical model of the temperature gradient of the mantle wedge beneath the central TMVB, I have determined that hydrous (3-7 wt% H_2O) partial melting at 11-14 kbar and 1190-1270°C, leaving a harzburgite residue, is the most likely origin of primitive high-Mg basaltic andesites and andesites in the Trans-Mexican Volcanic Belt.

APPENDIX

EPMA DATA

Table 9. EPMA Data for One-Atm Capsule Alloy Analyses

Run Product	Fe wt%	Au wt%	Pd wt%	Mn wt%	Ni wt%	Total
RMW-1 Capsule	1.23	70.47	27.04	*MDL*	0.01	99.08
	1.27	69.74	28.05	*MDL*	0.01	99.08
	1.14	69.46	27.83	*MDL*	*MDL*	98.43
	1.02	69.82	27.66	*MDL*	0.02	98.54
	0.87	70.39	27.27	*MDL*	*MDL*	98.54
RMW-2 Capsule	0.91	70.42	27.13	0.02	*MDL*	99.18
	0.94	70.31	27.95	0.00	*MDL*	99.18
	0.85	70.33	27.57	0.01	*MDL*	98.77
	0.74	70.37	27.25	0.02	*MDL*	98.41
	0.66	71.29	27.33	0.00	*MDL*	99.30
RMW-3 Capsule	0.95	71.32	27.43	*MDL*	0.02	98.54
	0.94	69.67	27.93	*MDL*	0.01	98.54
	0.83	70.37	27.77	*MDL*	0.01	98.99
	0.71	71.13	27.54	*MDL*	0.01	99.38
	0.60	70.98	27.37	*MDL*	*MDL*	98.93
RMW-4 Capsule	0.15	70.92	26.78	*MDL*	*MDL*	97.73
	0.14	70.96	26.63	*MDL*	*MDL*	97.73
	0.12	69.88	26.49	*MDL*	*MDL*	96.48
	0.10	71.49	26.93	*MDL*	*MDL*	98.55
	0.08	71.29	26.87	*MDL*	*MDL*	98.24
RMW-5 Capsule	0.12	71.72	27.11	*MDL*	*MDL*	99.25
	0.14	71.89	27.21	*MDL*	*MDL*	99.25
	0.10	71.86	27.24	*MDL*	*MDL*	99.21
	0.10	72.18	27.33	*MDL*	*MDL*	99.61
	0.09	72.01	27.04	*MDL*	*MDL*	99.13

Table 9. continued

Run Product	Fe wt%	Au wt%	Pd wt%	Mn wt%	Ni wt%	Total
RMW-6 Capsule	0.14	71.97	27.39	*MDL*	0.03	99.69
	0.17	71.94	27.58	*MDL*	0.01	99.69
	0.11	71.88	27.45	*MDL*	*MDL*	99.42
	0.09	71.87	27.52	*MDL*	*MDL*	99.45
	0.09	72.34	27.37	*MDL*	0.03	99.79
RMW-7 Capsule	0.89	70.70	26.82	*MDL*	*MDL*	98.40
	0.85	69.82	27.73	*MDL*	*MDL*	98.41
	0.62	70.42	27.35	*MDL*	*MDL*	98.41
	0.43	70.89	27.05	*MDL*	*MDL*	98.38
	0.26	71.46	27.00	*MDL*	*MDL*	98.73
RMW-8 Capsule	0.52	71.55	27.11	0.01	*MDL*	99.19
	0.51	70.83	27.87	0.01	0.02	99.23
	0.36	71.43	27.45	*MDL*	*MDL*	99.25
	0.23	71.77	27.33	*MDL*	*MDL*	99.33
	0.14	72.52	27.22	*MDL*	*MDL*	99.87
RMW-9 Capsule	0.43	72.25	27.29	*MDL*	*MDL*	99.98
	0.42	71.36	27.56	0.01	*MDL*	99.35
	0.29	72.03	27.40	0.02	*MDL*	99.73
	0.20	71.88	27.31	0.02	*MDL*	99.43
	0.14	71.67	27.07	*MDL*	*MDL*	98.86
RMW-10 Capsule	1.14	69.92	26.73	*MDL*	0.03	97.81
	1.12	70.07	27.05	*MDL*	*MDL*	98.21
	1.04	70.19	26.88	*MDL*	0.02	98.11
	0.96	70.43	26.74	*MDL*	*MDL*	98.13
	0.87	70.20	26.60	*MDL*	*MDL*	97.65
RMW-11 Capsule	0.93	70.97	26.86	*MDL*	0.03	98.78
	0.91	70.71	27.58	*MDL*	0.02	99.21
	0.81	71.13	27.24	*MDL*	*MDL*	99.14
	0.70	70.89	26.97	*MDL*	0.02	98.56
	0.61	71.83	26.97	*MDL*	0.01	99.42
RMW-12 Capsule	0.88	70.96	27.09	0.02	0.03	98.98
	0.88	70.33	27.51	0.02	0.01	98.75
	0.78	70.40	27.40	*MDL*	*MDL*	98.57
	0.67	71.17	27.22	*MDL*	*MDL*	99.05
	0.57	71.30	26.96	*MDL*	*MDL*	98.78

Table 9. continued

Run Product	Fe wt%	Au wt%	Pd wt%	Mn wt%	Ni wt%	Total
RMW-13 Capsule	1.91	71.95	26.66	*MDL*	0.04	100.56
	1.89	72.81	27.00	*MDL*	0.04	101.74
	1.29	70.93	26.18	*NA*	*NA*	98.41
	1.18	71.60	26.06	*NA*	*NA*	98.84
	1.10	71.76	25.94	*NA*	*NA*	98.81
	1.01	71.79	25.53	*NA*	*NA*	98.33
RMW-14 Capsule	0.96	72.23	27.06	*MDL*	*MDL*	100.24
	0.96	72.54	27.28	*MDL*	*MDL*	100.76
	1.02	71.91	25.47	*NA*	*NA*	98.40
	0.96	71.70	24.80	*NA*	*NA*	97.46
	0.94	72.14	25.21	*NA*	*NA*	98.29
	0.89	72.60	25.17	*NA*	*NA*	98.65
RMW-15 Capsule	0.77	72.38	27.16	*MDL*	0.03	100.35
	0.73	72.46	26.99	*MDL*	0.02	100.17
	0.78	71.91	26.06	*NA*	*NA*	98.75
	0.72	72.29	25.99	*NA*	*NA*	99.00
	0.66	71.82	25.60	*NA*	*NA*	98.09
	0.59	72.62	25.63	*NA*	*NA*	98.84
RMW-16 Capsule	0.24	70.85	27.05	*MDL*	0.02	98.14
	0.24	70.73	26.83	*MDL*	*MDL*	97.77
	0.17	71.92	26.66	*MDL*	0.03	98.77
	0.10	71.46	26.68	*MDL*	*MDL*	98.20
	0.08	70.90	26.76	*MDL*	*MDL*	97.69
RMW-17 Capsule	0.24	70.97	26.71	*MDL*	0.02	97.93
	0.21	70.96	27.16	*MDL*	0.01	98.33
	0.18	70.77	27.01	*MDL*	*MDL*	97.94
	0.10	71.32	27.08	*MDL*	*MDL*	98.46
	0.08	71.42	26.85	*MDL*	*MDL*	98.34
RMW-18 Capsule	0.20	71.45	26.88	*MDL*	*MDL*	98.54
	0.17	70.73	26.89	*MDL*	*MDL*	97.79
	0.13	71.26	27.10	*MDL*	*MDL*	98.48
	0.09	71.32	26.67	*MDL*	*MDL*	98.09
	0.05	71.38	27.00	*MDL*	*MDL*	98.45

NA not analyzed, *MDL* below minimum 99% detection limit

Table 10. EPMA Data for High-P Capsule Alloy Analyses

Run Product	Fe wt%	Au wt%	Pd wt%	Mn wt%	Ni wt%	Total
RW-1 Capsule	0.60	73.21	26.90	*MDL*	0.03	100.74
	0.60	73.29	26.99	*MDL*	0.04	100.89
	0.61	72.23	27.35	*MDL*	0.03	100.19
	0.58	73.41	26.67	*MDL*	0.03	100.69
	0.61	73.28	26.67	*MDL*	0.05	100.59
RW-2 Capsule	0.53	73.02	27.17	*MDL*	*MDL*	100.71
	0.59	73.22	27.00	*MDL*	0.01	100.82
	0.60	72.44	27.41	*MDL*	0.02	100.47
	0.55	72.88	26.84	*MDL*	0.02	100.26
	0.56	73.30	27.24	*MDL*	0.02	101.15
RW-3 Capsule	1.07	72.05	25.05	*NA*	*NA*	98.17
	1.11	72.26	25.29	*NA*	*NA*	98.67
	1.12	71.95	25.14	*NA*	*NA*	98.21
	1.16	71.46	24.98	*NA*	*NA*	97.60
	1.14	71.58	25.56	*NA*	*NA*	98.28
RW-4 Capsule	0.49	73.32	26.62	*MDL*	*MDL*	100.42
	0.47	73.05	26.92	*MDL*	0.01	100.45
	0.49	73.83	27.01	*MDL*	0.01	101.33
	0.50	73.30	26.91	*MDL*	0.02	100.73
	0.46	74.06	26.56	*MDL*	*MDL*	101.10
RW-6 Capsule	0.53	73.05	25.67	*NA*	*NA*	99.25
	0.53	72.69	25.44	*NA*	*NA*	98.66
	0.54	72.98	25.65	*NA*	*NA*	99.17
	0.54	73.47	25.66	*NA*	*NA*	99.67
	0.50	71.90	25.06	*NA*	*NA*	97.47
RW-7 Capsule	0.40	73.15	26.87	*NA*	*NA*	100.43
	0.41	73.27	26.65	*NA*	*NA*	100.33
	0.41	73.34	26.65	*NA*	*NA*	100.39
	0.42	72.87	26.93	*NA*	*NA*	100.23
	0.42	73.04	26.98	*NA*	*NA*	100.44
RW-8 Capsule	0.38	74.02	26.94	*NA*	*NA*	101.34
	0.40	73.82	26.72	*NA*	*NA*	100.95
	0.37	73.53	26.54	*NA*	*NA*	100.45
	0.42	73.50	26.60	*NA*	*NA*	100.53
	0.42	73.82	26.71	*NA*	*NA*	100.94

Table 10. continued

Run Product	Fe wt%	Au wt%	Pd wt%	Mn wt%	Ni wt%	Total
RW-9 Capsule	0.84	72.04	25.66	*NA*	*NA*	98.54
	0.82	71.75	25.66	*NA*	*NA*	98.23
	0.80	72.09	25.52	*NA*	*NA*	98.41
	0.83	72.06	25.79	*NA*	*NA*	98.68
	0.84	71.92	25.81	*NA*	*NA*	98.56
RW-10 Capsule	0.57	72.41	25.50	*NA*	*NA*	98.48
	0.56	72.25	25.58	*NA*	*NA*	98.40
	0.56	71.93	25.59	*NA*	*NA*	98.07
	0.56	72.15	25.57	*NA*	*NA*	98.29
	0.56	72.05	25.57	*NA*	*NA*	98.18
RW-11 Capsule	0.49	72.91	27.09	*NA*	*NA*	100.49
	0.50	73.60	27.08	*NA*	*NA*	101.18
	0.49	73.51	26.83	*NA*	*NA*	100.83
	0.48	73.66	26.43	*NA*	*NA*	100.57
	0.48	73.50	26.41	*NA*	*NA*	100.39
RW-13 Capsule	0.32	73.03	25.26	*NA*	*NA*	98.62
	0.29	72.61	25.23	*NA*	*NA*	98.12
	0.33	73.01	24.99	*NA*	*NA*	98.33
	0.31	73.32	25.12	*NA*	*NA*	98.75
	0.32	73.58	24.95	*NA*	*NA*	98.85
RW-16 Capsule	0.46	72.56	25.60	*NA*	*NA*	98.62
	0.46	72.37	25.60	*NA*	*NA*	98.43
	0.48	72.47	25.71	*NA*	*NA*	98.65
	0.47	72.68	25.55	*NA*	*NA*	98.70
	0.48	72.48	25.72	*NA*	*NA*	98.67
RW-17 Capsule	0.39	72.39	27.17	*NA*	*NA*	99.96
	0.38	72.83	27.01	*NA*	*NA*	100.23
	0.42	72.90	26.77	*NA*	*NA*	100.09
	0.38	72.52	26.94	*NA*	*NA*	99.84
	0.39	72.89	26.85	*NA*	*NA*	100.14
RW-18 Capsule	0.41	72.93	25.73	*NA*	*NA*	99.08
	0.43	73.01	25.61	*NA*	*NA*	99.05
	0.42	73.65	25.16	*NA*	*NA*	99.23
	0.41	73.22	25.44	*NA*	*NA*	99.07
	0.42	72.85	25.44	*NA*	*NA*	98.70

Table 10. continued

Run Product	Fe wt%	Au wt%	Pd wt%	Mn wt%	Ni wt%	Total
RW-19 Capsule	0.29	71.91	26.31	*NA*	*NA*	98.51
	0.29	72.73	26.54	*NA*	*NA*	99.56
	0.29	73.25	26.26	*NA*	*NA*	99.80
	0.29	73.07	26.43	*NA*	*NA*	99.78
	0.32	72.91	26.66	*NA*	*NA*	99.88
RW-20 Capsule	0.38	72.54	25.48	*NA*	*NA*	98.40
	0.39	72.80	25.64	*NA*	*NA*	98.83
	0.35	72.59	25.48	*NA*	*NA*	98.42
	0.39	72.13	25.35	*NA*	*NA*	97.87
	0.34	72.57	25.28	*NA*	*NA*	98.18
RW-22 Capsule	0.36	72.59	25.86	*NA*	*NA*	98.81
	0.35	72.62	25.77	*NA*	*NA*	98.74
	0.35	72.72	25.65	*NA*	*NA*	98.73
	0.36	72.29	25.70	*NA*	*NA*	98.35
	0.34	72.53	25.60	*NA*	*NA*	98.47
RW-24 Capsule	0.28	73.40	25.74	*NA*	*NA*	99.42
	0.26	73.58	25.53	*NA*	*NA*	99.37
	0.25	73.61	25.46	*NA*	*NA*	99.32
	0.25	73.98	25.37	*NA*	*NA*	99.60
	0.24	73.62	25.27	*NA*	*NA*	99.13
RW-25 Capsule	0.39	73.06	25.64	*NA*	*NA*	99.09
	0.39	72.89	25.59	*NA*	*NA*	98.88
	0.37	72.94	25.61	*NA*	*NA*	98.93
	0.37	73.20	25.66	*NA*	*NA*	99.23
	0.36	73.07	25.60	*NA*	*NA*	99.03

NA not analyzed, *MDL* below minimum 99% detection limit

Table 11. EPMA Data for One-Atm Glass Analyses

Run Product	SiO_2	TiO_2	Al_2O_3	Cr_2O_3	FeO_T[a]	NiO	MnO	MgO	CaO	Na_2O	K_2O	P_2O_5	H_2O[b]	Total
RMW-1 Glass	52.02	1.26	15.63	0.09	4.64	*NA*	0.17	11.71	11.64	2.42	0.10	0.12	0.00	99.81
	51.98	1.27	15.26	0.10	4.83	*NA*	0.13	12.66	11.42	2.40	0.09	0.12	0.00	100.27
	51.89	1.27	15.17	0.11	4.89	*NA*	0.17	12.68	11.58	2.42	0.09	0.11	0.00	100.35
	52.14	1.26	15.19	0.07	5.01	*NA*	0.14	12.64	11.28	2.22	0.09	0.12	0.00	100.16
	51.69	1.31	15.20	0.11	4.97	*NA*	0.15	12.68	11.39	2.28	0.10	0.11	0.00	100.01
	51.47	1.33	15.53	0.10	5.04	*NA*	0.17	12.67	11.06	2.26	0.09	0.10	0.00	99.82
	51.58	1.38	15.53	0.11	5.00	*NA*	0.18	12.67	10.96	2.29	0.09	0.09	0.00	99.88
	51.37	1.35	15.54	0.11	4.98	*NA*	0.15	12.69	11.35	2.34	0.09	0.11	0.00	100.08
	51.64	1.27	15.58	0.10	5.01	*NA*	0.19	12.65	11.62	2.30	0.09	0.10	0.00	100.56
	51.41	1.38	15.38	0.11	5.06	*NA*	0.20	12.66	10.85	2.39	0.09	0.10	0.00	99.62
RMW-2 Glass	55.76	0.76	17.84	0.09	3.02	*NA*	0.11	9.68	8.61	3.40	0.84	0.14	0.00	100.24
	55.41	0.80	17.80	0.10	3.03	*NA*	0.13	9.79	9.03	3.53	0.84	0.13	0.00	100.59
	55.20	0.84	17.76	0.07	3.16	*NA*	0.10	9.75	8.76	3.42	0.84	0.15	0.00	100.03
	55.68	0.85	17.76	0.06	3.16	*NA*	0.15	9.75	8.62	3.52	0.84	0.14	0.00	100.53
	55.37	0.81	17.83	0.07	3.19	*NA*	0.15	9.80	8.90	3.53	0.83	0.14	0.00	100.62
	55.35	0.76	17.90	0.09	3.34	*NA*	0.10	9.75	8.24	3.36	0.84	0.14	0.00	99.89
	55.35	0.82	17.75	0.09	3.24	*NA*	0.12	9.76	8.71	3.57	0.82	0.14	0.00	100.36
	55.19	0.78	17.84	0.06	3.21	*NA*	0.11	9.78	8.73	3.66	0.83	0.15	0.00	100.35
	55.37	0.82	17.79	0.08	3.28	*NA*	0.13	9.73	8.86	3.42	0.84	0.14	0.00	100.44
	55.69	0.81	17.87	0.05	3.19	*NA*	0.13	9.79	8.93	3.60	0.84	0.15	0.00	101.06

Table 11. continued

Run Product	SiO_2	TiO_2	Al_2O_3	Cr_2O_3	FeO_T[a]	NiO	MnO	MgO	CaO	Na_2O	K_2O	P_2O_5	H_2O[b]	Total
RMW-3 Glass	56.86	0.93	16.61	0.09	3.23	*NA*	0.11	10.13	8.22	3.67	0.99	0.13	0.00	100.97
	56.85	0.89	16.63	0.07	3.34	*NA*	0.13	10.19	8.08	3.56	1.00	0.16	0.00	100.91
	56.84	0.84	16.58	0.09	3.35	*NA*	0.12	10.18	7.91	3.57	1.02	0.14	0.00	100.64
	56.39	0.86	16.41	0.08	3.42	*NA*	0.16	10.18	8.12	3.60	1.00	0.14	0.00	100.34
	56.44	0.83	16.29	0.08	3.37	*NA*	0.14	10.20	8.08	3.58	1.01	0.15	0.00	100.16
	56.31	0.87	16.43	0.08	3.49	*NA*	0.16	10.21	7.88	3.67	0.99	0.15	0.00	100.23
	56.19	0.89	16.56	0.11	3.45	*NA*	0.13	10.04	8.04	3.73	1.00	0.16	0.00	100.30
	56.39	0.84	16.61	0.06	3.30	*NA*	0.11	10.14	7.83	3.50	1.01	0.15	0.00	99.93
	56.22	0.84	16.41	0.07	3.39	*NA*	0.11	10.12	7.88	3.51	1.01	0.15	0.00	99.70
	56.91	0.87	16.44	0.13	3.42	*NA*	0.16	10.07	8.07	3.55	1.02	0.14	0.00	100.78
RMW-4 Glass	48.92	1.25	14.53	0.06	9.34	*NA*	0.18	12.21	10.66	2.20	0.08	0.10	0.00	99.54
	48.49	1.23	14.53	0.10	9.61	*NA*	0.17	12.25	10.51	2.19	0.08	0.08	0.00	99.24
	48.30	1.21	14.45	0.08	9.41	*NA*	0.23	12.31	10.28	2.35	0.08	0.08	0.00	98.78
	48.15	1.24	14.56	0.06	9.40	*NA*	0.17	12.24	10.48	2.26	0.09	0.07	0.00	98.71
	47.87	1.18	14.60	0.09	9.37	*NA*	0.17	12.16	10.82	2.09	0.09	0.07	0.00	98.51
	48.66	1.19	14.37	0.05	9.46	*NA*	0.17	12.29	10.59	2.26	0.09	0.08	0.00	99.21
	48.29	1.18	14.57	0.07	9.32	*NA*	0.17	12.25	10.51	2.15	0.09	0.09	0.00	98.68
	48.46	1.16	14.57	0.08	9.32	*NA*	0.16	12.32	10.43	2.24	0.08	0.11	0.00	98.93
	48.74	1.20	14.34	0.11	9.37	*NA*	0.17	12.28	10.72	2.10	0.08	0.05	0.00	99.16

Table 11. continued

Run Product	SiO_2	TiO_2	Al_2O_3	Cr_2O_3	FeO_T[a]	NiO	MnO	MgO	CaO	Na_2O	K_2O	P_2O_5	H_2O[b]	Total
RMW-5 Glass	52.57	0.71	16.85	0.05	6.79	*NA*	0.11	9.15	8.27	3.44	0.81	0.12	0.00	98.85
	52.61	0.76	16.50	0.07	6.69	*NA*	0.13	9.11	8.17	3.16	0.79	0.12	0.00	98.11
	52.29	0.71	16.85	0.05	6.92	*NA*	0.15	9.02	8.06	3.56	0.79	0.14	0.00	98.54
	52.48	0.73	16.91	0.05	6.79	*NA*	0.14	9.05	7.97	3.42	0.79	0.13	0.00	98.46
	52.29	0.73	16.80	0.04	6.85	*NA*	0.14	8.99	8.32	3.27	0.79	0.15	0.00	98.37
	52.71	0.74	16.79	0.05	6.69	*NA*	0.14	9.05	8.12	3.37	0.79	0.15	0.00	98.61
RMW-6 Glass	54.06	0.77	15.57	0.03	6.53	*NA*	0.14	9.63	7.43	3.28	0.96	0.15	0.00	98.55
	54.21	0.83	15.67	0.08	6.72	*NA*	0.14	9.70	7.51	3.45	0.97	0.12	0.00	99.40
	53.99	0.80	15.64	0.06	6.68	*NA*	0.13	9.67	7.66	3.27	0.97	0.15	0.00	99.01
	54.23	0.85	15.53	0.08	6.73	*NA*	0.11	9.68	7.51	3.49	0.97	0.14	0.00	99.31
	53.89	0.78	15.68	0.08	6.81	*NA*	0.13	9.68	7.53	3.49	0.96	0.16	0.00	99.19
	54.13	0.78	15.85	0.07	6.85	*NA*	0.11	9.71	7.69	3.43	0.96	0.15	0.00	99.74
	54.15	0.79	15.71	0.07	6.73	*NA*	0.13	9.71	7.67	3.42	0.96	0.15	0.00	99.50
	53.97	0.82	15.56	0.07	6.76	*NA*	0.13	9.66	7.44	3.76	0.96	0.13	0.00	99.27
	53.95	0.80	15.63	0.07	6.74	*NA*	0.11	9.67	7.47	3.45	0.96	0.12	0.00	98.96
	54.19	0.78	15.70	0.05	6.80	*NA*	0.11	9.71	7.83	3.74	0.97	0.12	0.00	99.97
RMW-7 Glass	51.43	1.71	14.92	0.08	8.18	*NA*	0.20	8.15	12.57	2.72	0.09	0.11	0.00	100.17
	51.41	1.74	15.08	0.07	8.31	*NA*	0.20	8.11	12.84	2.63	0.10	0.12	0.00	100.61
	50.60	1.70	14.90	0.04	8.29	*NA*	0.22	8.26	12.35	2.72	0.10	0.12	0.00	99.31
	51.55	1.73	14.85	0.06	8.09	*NA*	0.21	8.16	12.83	2.48	0.10	0.12	0.00	100.17
	51.28	1.67	15.11	0.04	8.13	*NA*	0.19	8.15	12.32	2.59	0.10	0.09	0.00	99.68

Table 11. continued

Run Product	SiO_2	TiO_2	Al_2O_3	Cr_2O_3	FeO_T[a]	NiO	MnO	MgO	CaO	Na_2O	K_2O	P_2O_5	H_2O[b]	Total
RMW-8 Glass	55.65	0.96	16.80	0.02	6.63	*NA*	0.13	6.61	8.40	4.06	1.02	0.17	0.00	100.45
	55.30	0.97	17.06	0.04	6.88	*NA*	0.15	6.79	8.77	4.06	0.97	0.18	0.00	101.16
	55.72	0.98	16.89	0.01	6.64	*NA*	0.16	6.85	8.91	4.26	0.97	0.17	0.00	101.57
	55.19	0.99	17.04	0.04	6.89	*NA*	0.14	6.76	8.70	3.70	0.97	0.16	0.00	100.58
	55.28	0.98	16.86	0.03	6.86	*NA*	0.15	6.82	8.96	3.86	0.96	0.18	0.00	100.96
	55.44	1.00	17.00	0.01	6.82	*NA*	0.13	6.82	8.88	3.76	0.98	0.18	0.00	101.02
RMW-9 Glass	55.96	0.94	17.01	0.03	6.39	*NA*	0.12	6.80	8.53	4.05	1.03	0.16	0.00	101.01
	55.91	0.91	17.04	0.02	6.20	*NA*	0.12	6.76	8.42	3.89	1.04	0.16	0.00	100.48
	55.98	0.99	17.20	0.04	6.08	*NA*	0.13	6.86	8.61	3.81	1.03	0.16	0.00	100.89
	56.08	0.89	17.25	0.01	6.20	*NA*	0.15	6.92	8.80	3.94	1.03	0.15	0.00	101.41
	56.35	0.97	17.11	0.04	6.17	*NA*	0.16	6.84	8.31	3.93	1.04	0.16	0.00	101.09
	56.10	0.88	16.94	0.04	6.20	*NA*	0.13	6.86	8.76	3.96	1.03	0.16	0.00	101.07
	56.34	0.90	17.37	0.02	6.18	*NA*	0.11	6.75	8.55	3.90	1.03	0.16	0.00	101.31
	56.02	0.92	17.12	0.05	6.32	*NA*	0.15	6.76	8.64	3.94	1.04	0.16	0.00	101.11
RMW-10 Glass	50.97	1.33	15.46	0.07	5.84	*NA*	0.19	12.91	11.23	2.32	0.10	0.08	0.00	100.51
	51.38	1.33	15.43	0.12	5.83	*NA*	0.17	12.87	11.37	2.37	0.09	0.11	0.00	101.07
	51.19	1.34	15.32	0.10	5.89	*NA*	0.19	12.94	11.28	2.26	0.08	0.08	0.00	100.69
	51.26	1.31	15.46	0.13	5.76	*NA*	0.15	12.96	11.24	2.06	0.09	0.07	0.00	100.47
	51.36	1.32	15.50	0.15	5.86	*NA*	0.15	12.96	11.29	2.19	0.09	0.07	0.00	100.94
	51.55	1.26	15.43	0.13	5.85	*NA*	0.16	12.80	11.31	2.30	0.09	0.10	0.00	100.95
	51.46	1.28	15.40	0.11	5.88	*NA*	0.16	12.98	11.17	2.24	0.09	0.10	0.00	100.88
	51.39	1.33	15.46	0.09	5.77	*NA*	0.15	12.86	11.19	2.39	0.09	0.09	0.00	100.82
	51.43	1.31	15.25	0.09	5.83	*NA*	0.16	12.88	11.35	2.20	0.08	0.08	0.00	100.65
	51.56	1.33	15.32	0.11	5.87	*NA*	0.18	12.87	11.66	2.29	0.08	0.09	0.00	101.38

Table 11. continued

Run Product	SiO_2	TiO_2	Al_2O_3	Cr_2O_3	FeO_T[a]	NiO	MnO	MgO	CaO	Na_2O	K_2O	P_2O_5	H_2O[b]	Total
RMW-11 Glass	55.55	0.76	17.85	0.08	4.10	*NA*	0.12	9.48	8.76	3.50	0.85	0.16	0.00	101.19
	55.60	0.75	17.63	0.08	4.15	*NA*	0.12	9.38	8.78	3.50	0.85	0.15	0.00	100.98
	56.04	0.79	17.83	0.10	4.16	*NA*	0.13	9.39	8.44	3.39	0.84	0.15	0.00	101.26
	55.15	0.77	17.80	0.11	4.16	*NA*	0.12	9.47	8.95	3.65	0.84	0.13	0.00	101.13
	55.59	0.78	17.82	0.11	4.14	*NA*	0.10	9.45	8.62	3.51	0.85	0.14	0.00	101.11
	55.77	0.82	17.70	0.07	4.13	*NA*	0.14	9.46	8.74	3.49	0.84	0.15	0.00	101.30
	55.30	0.80	17.78	0.12	4.24	*NA*	0.13	9.45	8.62	3.40	0.84	0.15	0.00	100.81
	55.60	0.80	17.57	0.11	4.22	*NA*	0.14	9.35	8.65	3.43	0.84	0.13	0.00	100.85
	55.56	0.78	17.86	0.09	4.13	*NA*	0.14	9.48	8.54	3.41	0.85	0.14	0.00	100.98
	55.58	0.79	17.55	0.12	4.09	*NA*	0.11	9.46	8.66	3.37	0.84	0.13	0.00	100.69
RMW-12 Glass	56.75	0.89	16.52	0.07	3.88	*NA*	0.14	9.94	8.00	3.47	1.01	0.15	0.00	100.81
	57.06	0.87	16.31	0.09	3.88	*NA*	0.11	9.94	7.98	3.41	1.02	0.16	0.00	100.84
	56.78	0.90	16.49	0.11	3.91	*NA*	0.11	9.99	8.15	3.59	1.02	0.16	0.00	101.19
	56.56	0.87	16.37	0.10	3.94	*NA*	0.14	10.00	7.87	3.40	1.03	0.16	0.00	100.43
	56.86	0.84	16.60	0.07	3.97	*NA*	0.11	9.97	8.02	3.47	1.02	0.16	0.00	101.09
	56.46	0.82	16.46	0.10	4.08	*NA*	0.13	9.87	7.95	3.58	1.02	0.13	0.00	100.61
	56.62	0.84	16.34	0.08	4.11	*NA*	0.13	9.93	7.96	3.60	1.01	0.16	0.00	100.79
	56.28	0.84	16.38	0.07	4.06	*NA*	0.12	9.97	8.20	3.62	1.02	0.15	0.00	100.70
	56.47	0.83	16.37	0.10	3.94	*NA*	0.11	9.85	8.08	3.52	1.03	0.16	0.00	100.47
	56.12	0.82	16.53	0.09	4.05	*NA*	0.10	9.92	8.38	3.48	1.01	0.13	0.00	100.65

Table 11. continued

Run Product	SiO_2	TiO_2	Al_2O_3	Cr_2O_3	FeO_T[a]	NiO	MnO	MgO	CaO	Na_2O	K_2O	P_2O_5	H_2O[b]	Total
RMW-13 Glass	53.18	1.56	15.13	0.06	5.76	*NA*	0.16	8.10	11.56	2.62	0.13	0.19	0.00	98.44
	53.54	1.73	15.08	0.09	5.83	*NA*	0.17	8.06	11.79	2.80	0.13	0.17	0.00	99.39
	53.29	1.94	15.08	0.07	5.87	*NA*	0.19	8.05	11.70	2.74	0.12	0.19	0.00	99.23
	53.07	1.93	14.77	0.08	5.76	*NA*	0.20	8.03	11.65	2.81	0.13	0.20	0.00	98.62
	53.32	1.96	14.98	0.05	5.84	*NA*	0.19	8.01	11.41	2.78	0.13	0.18	0.00	98.85
	53.18	1.98	14.93	0.05	5.87	*NA*	0.17	8.06	11.66	2.79	0.13	0.18	0.00	99.02
	52.83	2.00	15.18	0.04	5.81	*NA*	0.19	7.93	11.29	2.73	0.13	0.18	0.00	98.31
RMW-14 Glass	56.36	1.07	16.66	0.03	4.85	*NA*	0.15	6.71	8.50	3.95	0.98	0.24	0.00	99.51
	56.42	1.03	16.32	0.04	4.81	*NA*	0.14	6.67	8.35	3.74	0.97	0.23	0.00	98.71
	56.26	1.07	16.58	0.04	4.84	*NA*	0.16	6.68	8.38	3.97	0.98	0.25	0.00	99.21
	56.54	0.97	16.56	0.05	4.91	*NA*	0.17	6.77	9.00	3.95	0.96	0.24	0.00	100.13
	57.95	0.88	16.51	0.03	4.47	*NA*	0.15	6.42	8.23	3.95	1.04	0.26	0.00	99.89
	56.07	0.91	16.22	0.01	4.75	*NA*	0.18	6.76	8.67	4.06	0.99	0.26	0.00	98.87
	56.09	0.90	16.55	0.05	4.78	*NA*	0.17	6.75	8.88	3.78	0.96	0.25	0.00	99.15
RMW-15 Glass	57.12	0.97	16.46	0.05	3.75	*NA*	0.12	6.54	8.57	3.84	1.10	0.24	0.00	98.76
	59.17	0.90	16.55	0.04	3.19	*NA*	0.10	6.04	7.66	3.87	1.22	0.26	0.00	99.01
	58.98	0.90	16.80	0.02	3.23	*NA*	0.10	6.16	7.84	4.23	1.21	0.24	0.00	99.72
	58.65	0.83	16.81	0.07	3.45	*NA*	0.13	6.40	8.02	4.38	1.18	0.24	0.00	100.16
	57.70	0.87	16.57	0.08	3.69	*NA*	0.15	6.50	8.50	3.85	1.12	0.28	0.00	99.31
	59.14	0.78	16.68	0.04	3.27	*NA*	0.11	6.26	7.71	4.23	1.21	0.22	0.00	99.66
	58.93	0.95	16.85	0.04	3.34	*NA*	0.14	6.30	8.04	4.21	1.21	0.22	0.00	100.22

Table 11. continued

Run Product	SiO_2	TiO_2	Al_2O_3	Cr_2O_3	FeO_T[a]	NiO	MnO	MgO	CaO	Na_2O	K_2O	P_2O_5	H_2O[b]	Total
RMW- 16 Glass	50.23	1.61	14.68	0.03	9.84	*NA*	0.19	7.90	11.55	2.59	0.11	0.13	0.00	98.85
	50.00	1.66	14.75	0.05	9.73	*NA*	0.19	7.99	12.08	2.65	0.10	0.09	0.00	99.30
	50.12	1.64	14.68	0.05	9.95	*NA*	0.18	7.98	12.03	2.64	0.10	0.12	0.00	99.48
	50.22	1.64	14.62	0.04	9.93	*NA*	0.20	7.99	11.60	2.54	0.10	0.13	0.00	99.01
	50.00	1.59	14.61	0.04	9.95	*NA*	0.20	7.92	11.94	2.51	0.10	0.12	0.00	98.97
	50.23	1.62	14.53	0.04	10.03	*NA*	0.21	7.95	11.98	2.33	0.10	0.10	0.00	99.13
	49.70	1.68	14.59	0.05	9.95	*NA*	0.20	7.98	12.03	2.54	0.11	0.09	0.00	98.92
	49.99	1.61	14.85	0.03	9.95	*NA*	0.17	7.96	11.72	2.63	0.10	0.10	0.00	99.11
	50.09	1.57	14.69	0.04	10.03	*NA*	0.18	7.96	11.87	2.65	0.11	0.13	0.00	99.33
RMW-17 Glass	53.64	0.82	19.35	0.03	9.84	*NA*	0.13	5.70	9.49	3.77	0.85	0.13	0.00	100.49
	54.43	0.94	16.89	0.06	9.73	*NA*	0.13	6.68	8.26	3.85	1.00	0.17	0.00	99.89
	54.48	0.98	16.91	0.05	9.95	*NA*	0.12	6.64	8.70	3.79	0.99	0.15	0.00	100.15
	54.09	0.95	16.87	0.05	9.93	*NA*	0.13	6.70	8.29	3.79	0.99	0.17	0.00	99.36
	54.37	0.99	16.97	0.02	9.95	*NA*	0.15	6.67	8.10	3.93	0.99	0.17	0.00	99.79
	54.39	0.98	16.97	0.00	10.03	*NA*	0.10	6.64	8.42	4.09	0.99	0.16	0.00	100.37
	54.17	0.94	16.71	0.03	9.95	*NA*	0.13	6.60	8.17	3.84	0.99	0.16	0.00	99.16
	53.88	0.97	16.94	0.05	9.95	*NA*	0.16	6.66	8.34	3.90	1.01	0.17	0.00	99.46
	54.17	0.94	16.94	0.04	10.03	*NA*	0.18	6.73	8.25	3.80	0.99	0.17	0.00	99.70

Table 11. continued

Run Product	SiO_2	TiO_2	Al_2O_3	Cr_2O_3	FeO_T[a]	NiO	MnO	MgO	CaO	Na_2O	K_2O	P_2O_5	H_2O[b]	Total
RMW-18 Glass	55.10	0.87	16.80	0.03	6.42	*NA*	0.15	6.39	8.28	3.51	1.08	0.17	0.00	98.80
	55.29	0.93	17.16	0.04	6.61	*NA*	0.12	6.64	8.24	3.84	1.05	0.16	0.00	100.09
	55.27	0.89	17.17	0.00	6.57	*NA*	0.11	6.60	8.22	3.79	1.06	0.16	0.00	99.84
	54.78	0.95	17.38	0.00	6.64	*NA*	0.16	6.38	8.28	3.82	1.08	0.16	0.00	99.63
	55.04	0.92	16.94	0.03	6.59	*NA*	0.11	6.74	8.30	3.82	1.05	0.17	0.00	99.70
	55.88	0.91	16.91	0.01	6.62	*NA*	0.15	6.65	8.28	4.07	1.08	0.16	0.00	100.73
	55.16	0.92	17.05	0.03	6.65	*NA*	0.13	6.58	8.59	3.90	1.08	0.17	0.00	100.26
	55.33	0.88	17.16	0.03	6.62	*NA*	0.13	6.50	8.31	3.80	1.07	0.18	0.00	100.01
	55.14	0.91	17.03	0.02	6.68	*NA*	0.11	6.63	8.24	3.60	1.06	0.18	0.00	99.58

Microprobe analyses in wt%

NA not analyzed, *MDL* below minimum 99% detection limit

[a] All FeO reported as FeO_T

[b] H_2O calculated iteratively by difference for RW glasses, adjusting ZAF corrections with each iteration

Table 12. EPMA Data for High-P Glass and Mineral Analyses

Run Product	SiO_2	TiO_2	Al_2O_3	Cr_2O_3	FeO_T[a]	NiO	MnO	MgO	CaO	Na_2O	K_2O	P_2O_5	H_2O[b]	Total
Glass Analyses														
RW-1 Glass	52.43	0.81	14.96	0.06	7.82	*MDL*	0.11	8.94	7.06	3.43	0.95	0.13	3.30	100.00
	51.49	0.82	15.02	0.09	7.79	*MDL*	0.14	8.97	7.37	3.49	0.94	0.13	3.74	100.00
	52.33	0.82	15.13	0.08	7.81	*MDL*	0.13	8.93	7.09	3.35	0.97	0.13	3.25	100.00
	52.86	0.78	15.16	0.07	7.83	*MDL*	0.09	8.93	7.24	2.76	0.94	0.13	3.21	100.00
	52.09	0.75	15.10	0.10	7.69	*MDL*	0.13	8.90	7.15	3.30	0.95	0.12	3.71	100.00
RW-2 Glass	51.57	0.89	15.76	0.06	7.39	*NA*	0.13	8.31	7.54	3.61	0.99	0.15	3.62	100.00
	52.01	0.91	15.43	0.04	7.41	*NA*	0.16	8.25	7.75	3.99	0.98	0.14	2.92	100.00
	52.50	0.86	15.37	0.05	7.47	*NA*	0.12	8.19	7.78	3.59	0.98	0.17	2.91	100.00
	52.16	0.86	15.25	0.04	7.53	*NA*	0.14	8.27	7.72	3.77	0.97	0.15	3.15	100.00
	52.15	0.88	15.44	0.05	7.58	*NA*	0.12	8.31	7.76	3.76	0.97	0.17	2.81	100.00
	52.38	0.84	15.28	0.02	7.32	*NA*	0.11	8.20	7.78	4.01	1.00	0.15	2.90	100.00
	52.26	0.87	15.68	0.03	7.10	*NA*	0.12	8.21	8.06	3.56	0.98	0.17	2.96	100.00
RW-3 Glass	54.23	0.99	17.69	0.02	6.28	*NA*	0.11	5.79	7.44	3.82	1.15	0.17	2.31	100.00
	54.51	0.99	17.36	0.05	6.22	*NA*	0.11	6.34	7.37	3.89	1.15	0.19	1.82	100.00
	54.08	0.96	17.45	0.04	6.21	*NA*	0.10	6.19	7.70	3.99	1.18	0.18	1.91	100.00
	54.47	0.99	17.54	0.03	6.17	*NA*	0.10	6.26	7.53	4.20	1.18	0.18	1.35	100.00
	54.33	0.93	17.43	0.03	6.38	*NA*	0.13	6.34	7.40	3.91	1.14	0.18	1.80	100.00
RW-4 Glass	50.58	0.75	14.44	0.11	7.86	*NA*	0.12	9.52	7.22	4.84	0.73	0.16	3.66	100.00
	50.20	0.82	14.35	0.07	7.83	*NA*	0.11	9.52	7.33	4.62	0.73	0.12	4.30	100.00
	50.55	0.78	14.42	0.05	7.78	*NA*	0.14	9.37	7.06	4.64	0.72	0.14	4.36	100.00
	50.88	0.74	14.63	0.06	7.61	*NA*	0.15	9.26	7.16	4.79	0.74	0.13	3.85	100.00

Table 12. continued

Run Product	SiO_2	TiO_2	Al_2O_3	Cr_2O_3	FeO_T[a]	NiO	MnO	MgO	CaO	Na_2O	K_2O	P_2O_5	H_2O[b]	Total
RW-6 Glass	52.31	0.78	15.10	0.08	7.94	0.01	0.10	9.49	7.13	3.29	0.92	0.12	2.74	100.00
	52.02	0.81	15.21	0.11	7.89	0.02	0.13	9.50	7.22	3.36	0.91	0.12	2.70	100.00
	52.64	0.73	15.08	0.07	7.93	0.02	0.10	9.47	7.50	3.30	0.90	0.12	2.14	100.00
	52.25	0.81	15.06	0.06	7.89	0.00	0.10	9.46	7.57	3.43	0.93	0.14	2.31	100.00
	51.98	0.77	15.26	0.09	8.07	0.02	0.08	9.54	7.42	3.24	0.91	0.12	2.50	100.00
	51.77	0.82	15.24	0.06	7.95	0.00	0.13	9.57	7.82	3.20	0.90	0.15	2.41	100.00
	51.50	0.79	15.22	0.07	8.02	0.00	0.11	9.63	7.38	3.40	0.93	0.12	2.82	100.00
RW-7 Glass	51.63	0.82	15.99	0.07	7.46	*NA*	0.11	8.70	7.08	3.87	0.95	0.15	3.17	100.00
	51.87	0.81	15.90	0.04	7.32	*NA*	0.13	8.59	7.48	3.41	0.89	0.15	3.39	100.00
	51.95	0.80	15.58	0.04	7.52	*NA*	0.14	8.64	7.37	3.80	0.96	0.17	3.04	100.00
	52.01	0.84	15.51	0.05	7.70	*NA*	0.11	8.75	7.37	3.68	0.94	0.16	2.87	100.00
	51.87	0.86	15.75	0.05	7.54	*NA*	0.12	8.68	7.37	3.67	0.96	0.14	2.99	100.00
	52.26	0.79	15.87	0.03	7.31	*NA*	0.14	8.66	7.18	3.83	0.96	0.14	2.84	100.00
	52.02	0.90	15.62	0.05	7.43	*NA*	0.13	8.68	7.61	3.52	0.95	0.16	2.93	100.00
RW-8 Glass	52.84	0.87	16.52	0.06	7.76	*NA*	0.12	7.46	7.80	3.75	1.03	0.16	1.63	100.00
	52.89	0.89	16.98	0.05	7.17	*NA*	0.14	7.50	7.77	3.73	1.03	0.15	1.71	100.00
	52.86	0.86	16.93	0.03	7.70	*NA*	0.12	7.56	7.57	3.56	1.03	0.17	1.62	100.00

Table 12. continued

Run Product	SiO_2	TiO_2	Al_2O_3	Cr_2O_3	FeO_T[a]	NiO	MnO	MgO	CaO	Na_2O	K_2O	P_2O_5	H_2O[b]	Total
RW-9 Glass	51.53	0.78	16.28	0.02	6.53	*MDL*	0.15	7.77	8.09	3.85	1.03	0.15	3.79	100.00
	52.05	0.87	16.22	0.06	6.52	*MDL*	0.13	7.80	7.80	4.02	1.04	0.15	3.33	100.00
	52.26	0.87	16.19	0.05	6.48	*MDL*	0.15	7.81	8.07	3.69	1.04	0.14	3.25	100.00
	52.00	0.85	16.06	0.05	6.47	*MDL*	0.14	7.78	8.34	4.03	1.03	0.12	3.12	100.00
	52.41	0.95	16.25	0.03	6.57	*MDL*	0.14	7.80	7.90	4.02	1.04	0.15	2.75	100.00
	52.10	0.90	16.31	0.07	6.50	*MDL*	0.13	7.75	8.13	3.95	1.04	0.14	2.99	100.00
	53.25	0.90	16.35	0.05	6.51	*MDL*	0.13	7.75	8.36	3.31	1.05	0.17	2.18	100.00
RW-10 Glass	52.71	0.75	15.16	0.06	7.46	0.01	0.13	9.54	7.28	3.27	0.92	0.14	2.56	100.00
	52.24	0.85	15.33	0.08	7.55	0.00	0.14	9.54	7.21	3.35	0.92	0.13	2.66	100.00
	52.44	0.82	15.21	0.06	7.53	0.03	0.14	9.56	7.39	3.42	0.93	0.14	2.32	100.00
	52.89	0.80	15.06	0.11	7.60	0.02	0.13	9.67	7.39	3.37	0.90	0.13	1.93	100.00
	53.04	0.78	14.91	0.06	7.63	0.01	0.14	9.70	7.24	3.39	0.91	0.15	2.04	100.00
	53.06	0.80	15.33	0.08	7.68	0.01	0.11	9.66	7.41	3.40	0.90	0.14	1.43	100.00
	53.26	0.82	14.93	0.06	7.44	0.01	0.11	9.53	7.44	3.25	0.92	0.16	2.08	100.00
RW-11 Glass	52.25	0.82	15.11	0.08	7.49	*NA*	0.10	9.09	7.59	3.56	0.93	0.14	2.83	100.00
	52.20	0.81	14.92	0.04	7.68	*NA*	0.10	9.03	7.29	3.50	0.92	0.15	3.35	100.00
	52.25	0.81	15.01	0.07	7.63	*NA*	0.12	9.09	7.13	3.32	0.93	0.16	3.46	100.00
	52.24	0.81	14.94	0.05	7.65	*NA*	0.14	9.08	7.11	3.56	0.85	0.12	3.45	100.00
RW-13 Glass	50.43	0.78	15.04	0.09	8.68	*NA*	0.15	9.07	7.09	3.45	0.83	0.14	4.25	100.00
	50.31	0.77	14.87	0.07	8.54	*NA*	0.12	9.08	7.07	3.46	0.83	0.12	4.76	100.00
	50.83	0.80	14.85	0.11	8.51	*NA*	0.13	9.08	6.36	3.65	0.88	0.14	4.68	100.00
	51.01	0.78	15.10	0.07	8.67	*NA*	0.12	9.11	7.10	2.87	0.88	0.15	4.14	100.00

Table 12. continued

Run Product	SiO_2	TiO_2	Al_2O_3	Cr_2O_3	FeO_T[a]	NiO	MnO	MgO	CaO	Na_2O	K_2O	P_2O_5	H_2O[b]	Total
RW-16 Glass	50.84	0.84	14.50	0.08	7.42	*NA*	0.12	9.27	7.00	4.00	0.77	0.14	5.03	100.00
	51.28	0.78	14.65	0.06	7.38	*NA*	0.11	9.25	7.01	4.35	0.79	0.14	4.20	100.00
	50.56	0.82	14.54	0.06	7.46	*NA*	0.14	9.43	7.24	4.45	0.72	0.12	4.46	100.00
	50.79	0.85	14.79	0.08	7.43	*NA*	0.14	9.34	6.96	4.46	0.78	0.14	4.24	100.00
RW-17 Glass	50.83	0.84	14.90	0.07	7.44	*NA*	0.12	9.20	7.07	4.48	0.78	0.15	4.12	100.00
	50.85	0.80	14.75	0.07	7.27	*NA*	0.12	9.15	7.12	4.45	0.79	0.14	4.48	100.00
	50.98	0.85	15.00	0.07	6.93	*NA*	0.14	9.11	6.98	4.56	0.79	0.14	4.45	100.00
RW-18 Glass	50.49	0.79	14.68	0.07	7.80	*NA*	0.13	9.49	7.01	4.35	0.79	0.14	4.27	100.00
	50.40	0.79	14.70	0.11	7.79	*NA*	0.13	9.48	7.01	4.49	0.78	0.14	4.19	100.00
	50.04	0.81	14.71	0.10	7.72	*NA*	0.08	9.54	7.02	4.52	0.78	0.15	4.52	100.00
RW-19 Glass	51.06	0.78	15.10	0.05	7.58	*NA*	0.10	8.36	7.02	4.36	0.79	0.15	4.65	100.00
	50.18	0.73	15.20	0.05	7.84	*NA*	0.12	8.40	7.26	4.97	0.84	0.15	4.27	100.00
	50.68	0.83	15.30	0.07	7.82	*NA*	0.11	8.34	7.01	4.35	0.84	0.13	4.53	100.00
	50.62	0.85	15.42	0.04	7.66	*NA*	0.13	8.37	7.14	4.52	0.82	0.14	4.29	100.00
RW-20 Glass	50.45	0.81	15.59	0.06	7.04	*NA*	0.12	7.62	7.10	4.94	0.76	0.15	5.37	100.00
	50.93	0.84	15.50	0.04	7.02	*NA*	0.13	7.65	7.32	5.02	0.74	0.13	4.68	100.00
	50.69	0.84	15.62	0.04	6.81	*NA*	0.10	7.62	7.12	5.01	0.74	0.12	5.30	100.00
	50.51	0.85	15.38	0.05	7.05	*NA*	0.13	7.65	7.21	4.93	0.73	0.14	5.37	100.00
	51.10	0.77	15.45	0.04	6.80	*NA*	0.14	7.66	7.41	5.19	0.71	0.14	4.58	100.00

Table 12. continued

Run Product	SiO_2	TiO_2	Al_2O_3	Cr_2O_3	FeO_T[a]	NiO	MnO	MgO	CaO	Na_2O	K_2O	P_2O_5	H_2O[b]	Total
RW-22 Glass	49.61	0.80	14.93	0.06	7.53	*NA*	0.15	7.98	7.17	3.49	0.92	0.12	7.25	100.00
	49.81	0.80	15.19	0.06	7.39	*NA*	0.13	7.95	7.34	3.07	0.90	0.15	7.22	100.00
	49.64	0.78	15.03	0.05	7.47	*NA*	0.13	7.95	6.88	3.16	0.82	0.16	7.92	100.00
	50.11	0.80	14.98	0.04	7.67	*NA*	0.14	8.03	7.08	3.24	0.87	0.17	6.87	100.00
	49.98	0.82	15.00	0.06	7.55	*NA*	0.16	8.04	7.21	3.46	0.88	0.16	6.69	100.00
	50.01	0.86	15.31	0.06	7.57	*NA*	0.14	8.02	7.38	3.13	0.85	0.15	6.52	100.00
	49.86	0.83	15.11	0.06	7.54	*NA*	0.12	8.02	7.26	3.14	0.88	0.14	7.05	100.00
RW-24 Glass	51.89	0.78	14.81	0.02	7.30	*MDL*	0.14	8.14	7.09	2.64	0.87	0.13	6.21	100.00
	51.84	0.76	14.97	0.00	7.33	*MDL*	0.12	8.00	7.27	1.86	0.87	0.14	6.81	100.00
	51.56	0.80	15.39	0.06	7.28	*MDL*	0.12	8.08	7.13	1.10	0.84	0.12	7.48	100.00
	51.97	0.76	14.76	0.05	7.21	*MDL*	0.10	8.12	7.22	2.55	0.88	0.11	6.25	100.00
	51.87	0.78	14.89	0.06	7.22	*MDL*	0.13	8.08	7.32	2.40	0.88	0.14	6.22	100.00
	51.48	0.76	15.04	0.04	7.29	*MDL*	0.13	8.13	6.82	2.25	0.88	0.13	7.06	100.00
	51.96	0.84	14.81	0.03	7.22	*MDL*	0.11	8.06	7.07	2.68	0.89	0.14	6.21	100.00
RW-25 Glass	52.39	0.75	14.65	0.08	7.71	0.01	0.16	9.36	7.06	3.60	0.91	0.13	3.19	100.00
	52.53	0.82	14.56	0.06	7.71	*MDL*	0.15	9.39	7.21	3.37	0.89	0.11	3.19	100.00
	52.09	0.83	14.68	0.08	7.73	0.01	0.12	9.46	7.54	3.48	0.90	0.13	2.94	100.00
	51.67	0.73	14.55	0.08	7.77	0.02	0.14	9.47	7.60	3.48	0.89	0.14	3.45	100.00
	51.97	0.67	14.58	0.06	7.79	*MDL*	0.12	9.45	7.46	3.48	0.88	0.12	3.43	100.00
	51.89	0.77	14.73	0.09	7.82	0.02	0.13	9.46	7.33	3.16	0.89	0.15	3.57	100.00
	51.53	0.79	14.83	0.06	7.73	0.02	0.11	9.49	7.34	3.51	0.90	0.13	3.56	100.00

Table 12. continued

Run Product	SiO_2	TiO_2	Al_2O_3	Cr_2O_3	FeO_T[a]	NiO	MnO	MgO	CaO	Na_2O	K_2O	P_2O_5	H_2O[b]	Total
RW Anhydrous	54.40	0.86	15.81	0.11	7.32	0.05	0.13	9.57	7.26	3.33	0.96	0.12	0.00	99.92
	54.66	0.88	15.67	0.07	7.30	0.03	0.12	9.53	7.67	3.26	0.95	0.12	0.00	100.27
	53.80	0.81	15.33	0.08	7.31	0.04	0.13	9.58	7.25	3.35	0.95	0.15	0.00	98.77
	54.28	0.86	15.49	0.09	7.38	0.02	0.13	9.52	7.57	3.30	0.95	0.14	0.00	99.74
	53.80	0.83	15.49	0.07	7.38	0.02	0.11	9.56	7.49	3.32	0.95	0.14	0.00	99.15
Mineral Analyses														
RW-2 Opx	54.25	0.08	5.52	0.53	8.06	*NA*	0.12	29.87	1.59	0.15	0.01	*MDL*	0.00	100.17
	54.79	0.09	4.74	0.48	8.29	*NA*	0.14	29.86	1.77	0.22	*MDL*	*MDL*	0.00	100.36
	55.52	0.10	3.74	0.41	7.92	*NA*	0.14	30.36	1.82	0.23	*MDL*	*MDL*	0.00	100.21
	54.01	0.07	5.19	0.65	7.94	*NA*	0.17	29.73	1.60	0.18	*MDL*	*MDL*	0.00	99.53
	54.51	0.06	5.18	0.56	7.86	*NA*	0.17	30.01	1.51	0.20	*MDL*	*MDL*	0.00	100.03
	54.27	0.12	5.03	0.60	7.94	*NA*	0.13	29.87	1.73	0.23	0.01	*MDL*	0.00	99.93
	54.88	0.10	5.18	0.52	7.94	*NA*	0.11	29.78	1.57	0.17	*MDL*	*MDL*	0.00	100.23
RW-2 Cpx	47.90	0.90	11.89	0.07	8.54	*NA*	0.20	14.34	13.19	1.32	0.03	0.12	0.00	98.50
	50.64	0.67	16.55	0.03	8.17	*NA*	0.17	12.65	10.93	1.13	0.09	0.09	0.00	101.13
RW-3 Opx	53.49	0.18	6.55	0.25	8.83	*NA*	0.17	28.36	2.04	0.36	0.04	0.01	0.00	100.28
	54.02	0.22	6.64	0.30	8.73	*NA*	0.17	27.61	2.05	0.24	0.05	*MDL*	0.00	100.01
	53.97	0.34	8.96	0.24	8.20	*NA*	0.14	24.18	3.12	0.67	0.13	0.02	0.00	99.96
	53.54	0.18	6.46	0.31	8.89	*NA*	0.18	28.44	1.85	0.22	0.02	*MDL*	0.00	100.10

Table 12. continued

Run Product	SiO_2	TiO_2	Al_2O_3	Cr_2O_3	FeO_T[a]	NiO	MnO	MgO	CaO	Na_2O	K_2O	P_2O_5	H_2O[b]	Total
RW-3 Cpx	50.60	0.37	9.05	0.21	7.91	*NA*	0.22	18.76	12.10	1.00	0.01	*MDL*	0.00	100.24
	52.09	0.31	6.76	0.33	8.06	*NA*	0.18	19.93	11.27	0.75	0.01	*MDL*	0.00	99.69
	51.44	0.31	7.26	0.12	8.19	*NA*	0.23	18.37	12.67	0.85	*MDL*	*MDL*	0.00	99.43
	51.65	0.33	6.69	0.38	7.54	*NA*	0.19	19.28	12.32	0.91	0.02	*MDL*	0.00	99.30
RW-7 Opx	53.79	0.14	4.26	0.87	7.44	*NA*	0.17	31.28	1.61	0.10	*MDL*	*MDL*	0.00	99.64
	54.22	0.12	4.21	0.77	7.48	*NA*	0.15	31.18	1.41	0.13	*MDL*	*MDL*	0.00	99.66
	54.75	0.09	3.97	0.81	7.94	*NA*	0.14	31.08	1.48	0.06	*MDL*	*MDL*	0.00	100.32
	55.02	0.11	3.83	0.72	7.81	*NA*	0.14	31.28	1.67	0.13	*MDL*	*MDL*	0.00	100.68
	54.72	0.10	4.04	0.61	7.59	*NA*	0.15	31.11	1.44	0.08	*MDL*	*MDL*	0.00	99.82
	55.07	0.12	3.86	0.65	7.74	*NA*	0.16	31.24	1.26	0.06	*MDL*	*MDL*	0.00	100.14
	54.30	0.12	4.50	0.85	7.55	*NA*	0.13	31.13	1.67	0.07	*MDL*	*MDL*	0.00	100.32
RW-8 Opx	54.22	0.16	4.71	0.56	8.13	*NA*	0.16	30.95	1.77	0.12	*MDL*	*MDL*	0.00	100.76
	54.34	0.15	4.54	0.52	9.01	*NA*	0.17	30.49	1.71	0.08	0.01	*MDL*	0.00	101.00
	56.67	0.10	1.95	0.44	8.02	*NA*	0.16	32.06	1.37	0.09	0.01	*MDL*	0.00	100.86
RW-8 Cpx	53.49	0.92	17.42	0.05	8.15	*NA*	0.13	6.52	7.96	2.68	0.81	0.17	0.00	98.30
	53.14	0.93	17.63	0.04	7.86	*NA*	0.10	6.26	7.95	2.43	0.83	0.18	0.00	97.36
	53.78	0.96	18.31	0.01	7.74	*NA*	0.12	5.63	8.30	2.65	0.78	0.20	0.00	98.47
	53.97	0.95	18.29	0.02	7.17	*NA*	0.14	5.74	8.12	4.61	0.84	0.17	0.00	100.02
	53.27	0.93	18.37	0.03	6.57	*NA*	0.12	6.00	7.60	4.02	0.83	0.18	0.00	97.92

Table 12. continued

Run Product	SiO_2	TiO_2	Al_2O_3	Cr_2O_3	FeO_T[a]	NiO	MnO	MgO	CaO	Na_2O	K_2O	P_2O_5	H_2O[b]	Total
RW-9 Olivine	38.75	0.04	0.03	0.05	12.35	0.11	0.17	47.43	0.22	*MDL*	*MDL*	*MDL*	0.00	99.16
	38.46	0.00	0.04	0.04	12.19	0.09	0.20	47.60	0.20	*MDL*	*MDL*	*MDL*	0.00	98.82
	39.08	-0.01	0.03	0.04	12.28	0.10	0.18	47.60	0.19	*MDL*	*MDL*	*MDL*	0.00	99.46
	38.76	0.02	0.05	0.01	12.01	0.08	0.16	47.63	0.17	*MDL*	*MDL*	*MDL*	0.00	98.91
	38.74	0.03	0.04	0.01	12.26	0.10	0.17	47.38	0.21	*MDL*	*MDL*	*MDL*	0.00	98.97
	39.16	0.03	0.03	0.05	12.26	0.11	0.19	47.36	0.16	*MDL*	*MDL*	*MDL*	0.00	99.34
	38.40	0.00	0.06	0.04	12.20	0.12	0.16	47.59	0.22	*MDL*	*MDL*	*MDL*	0.00	98.78
RW-9 Opx	53.99	0.16	3.83	0.83	8.18	*NA*	0.16	30.51	1.63	0.04	*MDL*	*MDL*	0.00	99.33
	54.03	0.16	4.27	0.80	8.25	*NA*	0.17	30.51	1.78	0.05	*MDL*	*MDL*	0.00	100.02
	54.50	0.15	3.26	0.63	8.08	*NA*	0.15	30.84	2.04	0.08	*MDL*	*MDL*	0.00	99.73
	53.89	0.17	3.58	0.78	8.05	*NA*	0.19	30.60	1.94	0.07	*MDL*	*MDL*	0.00	99.25
	54.58	0.16	3.06	0.52	7.68	*NA*	0.17	31.07	1.57	0.10	*MDL*	*MDL*	0.00	98.92
	54.08	0.14	3.94	0.78	8.16	*NA*	0.20	30.66	1.71	0.08	*MDL*	*MDL*	0.00	99.71
	55.52	0.11	2.16	0.37	7.98	*NA*	0.14	31.59	1.76	0.04	*MDL*	*MDL*	0.00	99.65
RW-11 Olivine	39.72	0.03	0.04	0.05	10.83	0.36	0.13	48.66	0.18	*MDL*	*MDL*	0.03	0.00	100.04
	39.89	0.01	0.05	0.05	11.44	0.18	0.16	48.12	0.15	*MDL*	*MDL*	0.01	0.00	100.06
	39.51	0.01	0.03	0.06	11.55	0.18	0.15	48.15	0.13	*MDL*	*MDL*	0.02	0.00	99.80
	40.45	0.00	0.02	0.03	10.97	0.37	0.13	48.64	0.17	*MDL*	*MDL*	*MDL*	0.00	100.80
	40.60	0.02	0.03	0.07	10.54	0.41	0.17	48.99	0.18	*MDL*	*MDL*	0.05	0.00	101.07
	39.97	0.03	0.05	0.07	10.48	0.43	0.12	48.87	0.15	*MDL*	*MDL*	0.02	0.00	100.19
	39.88	0.03	0.04	0.07	11.23	0.25	0.12	48.26	0.16	*MDL*	*MDL*	0.01	0.00	100.05

Table 12. continued

Run Product	SiO_2	TiO_2	Al_2O_3	Cr_2O_3	FeO_T[a]	NiO	MnO	MgO	CaO	Na_2O	K_2O	P_2O_5	H_2O[b]	Total
RW-17 Opx	54.60	0.10	3.29	0.91	7.68	*NA*	0.17	31.87	1.30	0.05	*MDL*	*MDL*	0.00	99.96
	54.47	0.11	3.52	0.87	7.26	*NA*	0.16	31.64	1.30	0.08	*MDL*	*MDL*	0.00	99.36
	55.22	0.09	3.45	0.89	7.71	*NA*	0.15	31.63	1.48	0.03	*MDL*	*MDL*	0.00	100.67
	54.70	0.10	3.61	0.92	7.66	*NA*	0.14	31.81	1.32	0.04	*MDL*	*MDL*	0.00	100.29
	54.84	0.11	4.19	0.91	7.51	*NA*	0.17	31.84	1.38	0.10	*MDL*	*MDL*	0.00	101.03
	54.95	0.08	3.65	0.93	7.62	*NA*	0.17	31.79	1.29	0.03	*MDL*	*MDL*	0.00	100.52
RW-19 Opx	54.26	0.10	4.08	0.73	7.53	*NA*	0.14	31.59	1.29	0.10	0.01	*MDL*	0.00	99.83
	54.66	0.11	3.63	0.65	8.02	*NA*	0.17	31.33	1.33	0.08	0.01	*MDL*	0.00	99.96
	54.44	0.10	4.04	0.90	7.11	*NA*	0.17	31.52	1.50	0.10	*MDL*	*MDL*	0.00	99.86
	54.54	0.13	3.61	0.62	7.60	*NA*	0.17	31.55	1.32	0.05	0.01	*MDL*	0.00	99.62
	55.18	0.11	3.39	0.61	8.09	*NA*	0.16	31.37	1.32	0.13	0.01	*MDL*	0.00	100.37
	54.87	0.08	3.45	0.60	7.93	*NA*	0.17	31.33	1.36	0.05	0.01	*MDL*	0.00	99.83
	54.71	0.10	3.84	0.63	7.28	*NA*	0.17	31.22	1.38	0.09	*MDL*	*MDL*	0.00	99.41
RW-20 Olivine	38.78	0.07	0.23	0.04	12.69	0.27	0.15	46.02	0.21	*MDL*	0.02	*MDL*	0.00	98.52
	38.69	0.00	0.02	0.01	12.59	0.31	0.17	46.99	0.08	*MDL*	*MDL*	*MDL*	0.00	98.85
	38.78	-0.01	0.01	0.00	11.89	0.35	0.16	47.76	0.11	*MDL*	*MDL*	*MDL*	0.00	99.05
	38.73	0.00	0.03	0.02	12.12	0.36	0.12	47.54	0.16	*MDL*	0.01	*MDL*	0.00	99.11
	38.84	0.02	0.02	0.06	12.48	0.30	0.18	46.92	0.17	*MDL*	*MDL*	*MDL*	0.00	99.01
	39.17	0.07	0.02	0.03	12.51	0.27	0.18	46.69	0.14	*MDL*	*MDL*	*MDL*	0.00	99.21

Table 12. continued

Run Product	SiO_2	TiO_2	Al_2O_3	Cr_2O_3	FeO_T[a]	NiO	MnO	MgO	CaO	Na_2O	K_2O	P_2O_5	H_2O[b]	Total
RW-20 Opx	57.20	0.09	1.44	0.52	7.91	*NA*	0.17	32.00	1.37	0.03	*MDL*	*MDL*	0.00	100.73
	57.23	0.08	1.50	0.47	7.99	*NA*	0.16	32.00	1.43	0.06	*MDL*	*MDL*	0.00	100.94
	56.73	0.09	1.50	0.45	8.07	*NA*	0.18	32.10	1.55	0.05	*MDL*	*MDL*	0.00	100.68
	57.29	0.08	1.43	0.44	8.20	*NA*	0.21	32.09	1.42	0.06	*MDL*	*MDL*	0.00	101.21
	57.00	0.07	1.49	0.47	8.10	*NA*	0.16	32.06	1.31	0.02	*MDL*	*MDL*	0.00	100.67
RW-22 Opx	55.17	0.14	3.68	0.53	7.56	*NA*	0.16	31.55	1.18	0.05	*MDL*	*MDL*	0.00	100.02
	54.75	0.12	4.33	0.37	7.60	*NA*	0.16	31.27	1.42	0.09	*MDL*	*MDL*	0.00	100.08
	54.78	0.16	3.79	0.34	7.56	*NA*	0.16	31.30	1.68	0.07	*MDL*	*MDL*	0.00	99.83
	55.01	0.08	3.22	0.76	8.32	*NA*	0.17	31.30	1.17	0.09	*MDL*	*MDL*	0.00	100.09
	54.70	0.14	3.83	0.39	7.65	*NA*	0.14	31.22	1.56	0.03	*MDL*	*MDL*	0.00	99.63
	54.57	0.09	4.64	0.48	7.72	*NA*	0.15	31.17	1.35	0.06	*MDL*	*MDL*	0.00	100.23
	54.53	0.13	4.07	0.73	7.59	*NA*	0.16	31.09	1.58	0.07	*MDL*	*MDL*	0.00	99.97
RW-24 Olivine	39.43	0.02	0.02	0.07	11.52	0.29	0.17	48.11	0.13	*MDL*	*MDL*	*MDL*	0.27	100.00
	40.51	0.00	0.04	0.08	11.48	0.32	0.17	47.97	0.12	*MDL*	*MDL*	*MDL*	0.00	100.69
	40.05	0.00	0.01	0.07	11.45	0.34	0.19	48.32	0.17	*MDL*	*MDL*	*MDL*	0.00	100.57
	40.13	0.05	0.01	0.03	12.03	0.27	0.16	47.62	0.17	*MDL*	*MDL*	*MDL*	0.00	100.46
	39.32	-0.03	0.03	0.02	11.96	0.24	0.14	47.79	0.13	*MDL*	*MDL*	*MDL*	0.39	100.00
	39.92	0.02	0.03	0.01	11.59	0.27	0.15	47.93	0.12	*MDL*	*MDL*	*MDL*	0.00	100.03
	39.94	0.01	0.06	0.01	12.31	0.30	0.21	47.13	0.16	*MDL*	*MDL*	*MDL*	0.00	100.15
	39.01	0.04	0.02	0.02	11.59	0.37	0.18	47.71	0.15	*MDL*	*MDL*	*MDL*	0.91	100.00

Table 12. continued

Run Product	SiO_2	TiO_2	Al_2O_3	Cr_2O_3	FeO_T[a]	NiO	MnO	MgO	CaO	Na_2O	K_2O	P_2O_5	H_2O[b]	Total
RW-24 Opx	55.76	0.07	3.00	1.05	7.95	0.07	0.14	31.92	1.15	0.04	*MDL*	*MDL*	0.00	101.11
	55.78	0.15	2.88	0.92	7.99	0.07	0.19	31.70	1.34	0.05	*MDL*	*MDL*	0.00	101.06
	55.46	0.12	2.93	1.03	7.89	0.09	0.15	31.75	1.27	0.04	*MDL*	*MDL*	0.00	100.73
	56.40	0.09	1.30	0.55	7.63	0.06	0.15	32.86	1.42	0.03	*MDL*	*MDL*	0.00	100.49
	57.12	0.09	1.23	0.61	7.63	0.06	0.17	32.83	1.45	0.04	*MDL*	*MDL*	0.00	101.19
	55.85	0.07	3.06	0.99	7.88	0.05	0.13	31.84	1.26	0.04	*MDL*	*MDL*	0.00	101.16

Microprobe analyses in wt%

NA not analyzed, *MDL* below minimum 99% detection limit

[a] All Fe reported as FeO_T

[b] H_2O calculated iteratively by difference for RW glasses, adjusting ZAF corrections with each iteration

REFERENCES

Brandon, A. D. & Draper, D. S. (1996). Constraints on the origin of the oxidation state of the mantle overlying subduction zones: An example from Simcoe, Washington, USA. *Geochimica et Cosmochimica Acta* **60**, 1739-1749, doi:10.1016/0016-7037(96)00056-7.

Carmichael, I. S. E. (1991). The redox states of basic and silicic magmas: a reflection of their source regions? *Contributions to Mineralogy and Petrology* **106**, 129-141, doi:10.1007/BF00306429.

Cervantes, P. & Wallace, P. J. (2003). Role of H_2O in subduction-zone magmatism: new insights from melt inclusions in high-Mg basalts from central Mexico. *Geology* **31,** 235-238, doi:10.1130/0091-7613(2003)031<0235.

Christie, D. M., Carmichael, I. S. E. & Langmuir C. H. (1986). Oxidation states of mid-ocean ridge basalt glasses. *Earth and Planetary Science Letters* **79**, 297-411, doi:10.1016/0012-821X(86)90195-0.

Crawford, A. J., Falloon, T. J. & Green, D. H. (1989). Classification, petrogenesis and tectonic setting of boninites. In: Crawford, A. J. (ed) *Boninites and Related Rocks.* London: Unwin Hyman, pp. 1-49.

Defant, M. J. & Drummond, M. S. (1990). Derivation of some modern arc magmas by melting of young subducted lithosphere. *Nature* **347**, 662–65.

Eugster, H. P. & Wones, D. R. (1962). Stability Relations of the ferruginous biotite, annite. *Journal of Petrology* **3**, 82-125.

Gaetani, G. A. & Grove, T. L. (2003). Experimental constraints on melt generation in the mantle wedge. In: Eiler, J. (ed) *Inside the Subduction Factory, American Geophysical Monograph* **138**, 107-133, doi:10.1029/138GM07.

Gaetani, G. A. & Grove, T. L. (1998). The influence of water on melting of mantle peridotite. *Contributions to Mineralogy and Petrology* **131**, 323-346, doi:10.1007/s004100050396.

Ghiorso, M. S., Hirschmann, M. M., Reiners, P. W. & Kress, V. C. III (2002). The pMELTS: a revision of MELTS aimed at improving calculation of phase relations and major element partitioning involved in partial melting of the mantle at pressures up to 3 GPa. *Geochemistry Geophysics Geosystems* **3**, 1030, doi:10.1029/2001GC000217.

Gómez-Tuena, A., Langmuir, C. H., Goldstein, S. L., Straub, S. M. & Ortega-Gutiérrez, F. (2007). Geochemical Evidence for Slab Melting in the Trans-Mexican Volcanic Belt. *Journal of Petrology* **48**, 537-562, doi:10.1093/petrology/egl071.

Grove, T. L., Chatterjee, N., Parman, S. W. & Médard, E. (2006). The influence of H_2O on mantle wedge melting. *Earth and Planetary Science Letters* **249**, 74-89, doi:10.1016/j.epsl.2006.06.043.

Grove, T. L., Elkins-Tanton, L. T., Parman, S. W., Chatterjee, N., Müntener, O. & Gaetani, G. A. (2003). Fractional crystallization and mantle-melting controls on calc-alkaline differentiation trends. *Contributions to Mineralogy and Petrology* **145**, 515-533, doi:10.1007/s00410-003-0448-z.

Grove, T. L., Parman, S. W., Bowring, S. A., Price, R. C. & Baker, M. B. (2002). The role of an H2O-rich fluid component in the generation of primitive basaltic andesites and andesites from the Mt. Shasta region, N California. *Contributions to Mineralogy and Petrology* **142**, 375–396.

Grove, T. L. (1981). Use of FePt alloys to eliminate the iron loss problem in 1 atmosphere gas mixing experiments: theoretical and practical considerations. *Contributions to Mineralogy and Petrology* **78**, 298-304, doi:10.1007/BF00398924.

Guilbaud, M., Siebe, C. & Agustín-Flores, J. (2009). Eruptive style of the young high-Mg basaltic-andesite Pelagatos scoria cone, southeast of México City. *Bulletin of Volcanology* **71**, 859–880, doi:10.1007/s00445-009-0271-0.

Haggerty, S. E. (1976) Opaque mineral oxides in terrestrial igneous rocks. In: Ruble, D. H. III (ed.) *Oxide Minerals, MSA Short Course Notes* **3**, 101-300.

Hasenaka, T. & Carmichael, I. S. E. (1987) The Cinder Cones of Michoacán-Guanajuato, Central Mexico: Petrology and Chemistry. *Journal of Petrology* **28**, 241-269.

Hebert, R., Bideau, D. & Hekinian, R. (1983). Ultramafic and mafic rocks from the Garrett Transform near 13°30'S on the East Pacific Rise: igneous petrology. *Earth and Planetary Science Letters* **65**, 107-125, doi:10.1016/0012-821X(83)90193-0.

Hirose, K. (1997). Melting experiments of lherzolite KLB-1 under hydrous conditions and generation of high-magnesian andesitic melts. *Geology* **25**, 42-44, doi:10.1130/0091-7613(1997)025<0042.

Huebner, J. S. & Sato, M. (1970). The oxygen fugacity-temperature relationships of manganese oxide and nickel oxide buffers. *American Mineralogist* **55**, 934-952.

Johnson, E. R., Wallace, P. J., Granados, H. D., Manea, V. C., Kent, A. J. R., Bindeman, I. N. & Donegan, C. S. (2009). Subduction-related Volatile Recycling and Magma Generation beneath Central Mexico: Insights from Melt Inclusions, Oxygen Isotopes and Geodynamic Models. *Journal of Petrology* **50**, 1729-1764, doi:10.1093/petrology/egp051.

Johnston, A. D. (1986). Anhydrous P-T phase relations of near-primary high-alumina basalt from the South Sandwich Islands. *Contributions to Mineralogy and Petrology* **92**, 368-382, doi:10/1007/BF00572166.

Kägi, R., Müntener, O., Ulmer, P. & Ottolini, L. (2005). Piston-cylinder experiments on H_2O undersaturated Fe-bearing systems: An experimental setup approaching fO_2 conditions of natural calc-alkaline magmas. *American Mineralogist* **90**, 708-717, doi:10.2138/am2005.1663.

Kelemen, P. B. (1995). Genesis of high Mg# andesites and the continental crust. *Contributions to Mineralogy and Petrology* **120**, 1-19, doi:10.1007/BF00311004.

Kelemen, P. B., Rilling, J. L., Parmentier, E. M., Mehl, L. & Hacker, R. (2003). Thermal Structure due to Solid-State Flow in the Mantle Wedge Beneath Arcs. In: Eiler, J. (ed) *Inside the Subduction Factory, American Geophysical Monograph* **138**, 293-311.

Kelley, K. A., Plank, T., Grove, T. L., Stopler, E. M., Newman, S. & Hauri, E. (2006). Mantle melting as a function of water content beneath back-arc basins. *Journal of Geophysical Research* **111**, B09208, doi:10.1029/2005JB003732.

Kessell, R., Beckett, J. R. & Stolper, E. M. (2001). Thermodynamic properties of the Pt-Fe system. *American Mineralogist* **86**, 1003-1014.

Kress, V. C. & Carmichael, I. S. E. (1991). The compressibility of silicate liquids containing Fe_2O_3 and the effect of composition, temperature, oxygen fugacity and pressure on their redox states. *Contributions to Mineralogy and Petrology* **108**, 82-92, doi:10.1007/BF00307328.

Langmuir, C. H., Klein, E. M. & Plank, T. (1992). Petrological systematics of mid-ocean ridge basalts: Constraints on melt generation beneath ocean ridges. In: Morgan, J. P., Blackman, D. K. & Sinton, J.M. (eds) *Mantle Flow and Melt Generation at Mid-Ocean Ridges, Geophysical Monograph Series* **71**, 183–280.

Lee, C. A., Luffi, P., Plank, T., Dalton, H. & Leeman, W. P. (2009). Constraints on the depths and temperatures of basaltic magma generation on Earth and other terrestrial planets using new thermobarometers for mafic magmas. *Earth and Planetary Science Letters* **279**, 20-33, doi:10.1016/j.epsl.2008.12.020.

Lee, C. A., Leeman, W. P., Canil, D. & Li, Z. A. (2005). Similar V/Sc systematics in MORB and arc basalts: Implications for the oxygen fugacities of their mantle source regions. *Journal of Petrology* **46**, 2313-2336, doi:10.1093/petrology/egi056.

Manea, V. C. & Manea, M. (in review). Flat-slab thermal structure and evolution beneath Central Mexico. *Pure and Applied Geophysics.*

Manea, V. C., Manea, M., Kostoglodov, V. & Sewell, G., (2005). Thermo-mechanical model of the mantle wedge in Central Mexican subduction zone and a blob tracing approach for the magma transport. *Physics of the Earth and Planetary Interiors* **149**, 165-186, doi:10.1016/j.pepi.2004.08.024.

Médard, E., Grove, T. L. (2008). The effect of H_2O on the olivine liquidus of basaltic melts: experiments and thermodynamic models. *Contributions to Mineralogy and Petrology* **155**, 417-432, doi:10.1007/s00410-007-0250-4.

Meriggi, L., Macías, J. L., Tommasini, S., Capra, L. & Conticelli, S. (2008). Heterogeneous magmas of the Quaternary Sierra Chichinautzin volcanic field (central Mexico): the role of an amphibole-bearing mantle and magmatic evolution processes. *Revista Mexicana de Ciencias Geológicas* **25**, 197-216.

Nielsen, C. H. & Sigurdsson, H. (1981). Quantitative methods for electron microprobe analysis of sodium in natural and synthetic glasses. *American Mineralogist* **66**, 547-552.

Pardo, M. & Suárez, G. (1995). Shape of the subducted Rivera and Cocos plates in southern Mexico: seismic and tectonic implications. *Journal of Geophysical Research* **100**, 12357-12373.

Parkinson, I. J. & Arculus, R. J. (1999). The redox state of subduction zones: insights from arc-peridotites. *Chemical Geology* **160**, 409-423, doi:10.1016/S0009-2541(99)00110-2.

Parman, S. W. & Grove, T. L. (2004). Harzburgite melting with and without H_2O: Experimental data and predictive modeling. *Journal of Geophysical Research* **109**, doi:10.1029/2003JB002566.

Peacock S. M. (2003). Thermal structure and metamorphic evolution of subducting slabs. In: Eiler, J. (ed) *Inside the Subduction Factory, American Geophysical Monograph* **138**, 7-21.

Peréz-Campos, X., Kim, Y., Husker, A., Davis, P. M., Clayton, R. W., Iglesias, A., Pacheco, J. F., Singh, S. K., Manea, V. C. & Gurnis, M. (2008). Horizontal subduction and truncation of the Cocos Plate beneath central Mexico. *Geophysical Research Letters* **35**, L18303, doi:10.1029/2008GL035127.

Pickering, J. M., Schwab, B. E., Johnston, A. D. (1998). Off-center hot spots: double thermocouple determination of the thermal gradient in a 1.27 cm (1/2 in.) CaF_2 piston-cylinder furnace assembly. *American Mineralogist* **83**, 228-235.

Roman, D. C., Cashman, K. V., Gardner, C. A., Wallace, P. J. & Donovan, J. J. (2006). Storage and interaction of compositionally heterogeneous magmas from the 1986 eruption of Augustine Volcano, Alaska. *Bulletin of Volcanology* **68**, 240-254, doi:10.1007/s00445-005-0003-z.

Schaaf, P., Stimac, J., Siebe, C. & Macías, J. L. (2005). Geochemical Evidence for Mantle Origin and Crustal Processes in Volcanic Rocks from Popocatepetl and Surrounding Monogenetic Volcanoes, Central Mexico. *Journal of Petrology* **46**, 1243-1282, doi:10.1093/petrology/egi015.

Straub, S. M., LaGatta, A. B., Martin-Del Pozzo, A. L. & Langmuir, C. H. (2008). Evidence from high-Ni olivines for a hybridized peridotite/pyroxenite source for orogenic andesites from the central Mexican Volcanic Belt. *Geochemistry Geophysics Geosystems* **9**, Q030007, doi:10.1029/2007GC001583.

Stolper, E. & Newman, S. (1994). The role of water in the petrogenesis of Mariana trough magmas. *Earth and Planetary Science Letters* **121**, 293-325, doi:10.1016/0012-821X(94)90074-4.

Tatsumi, Y. (2006). High-Mg Andesites in the Setouchi Volcanic Belt, Southwestern Japan: Analogy to Archean Magmatism and Continental Crust Formation? *Annual Review of Earth and Planetary Sciences* **34**, 467-499, doi:10.1146/annurev.earth.34.031405.125014.

Tatsumi, Y. & Ishizaka, K. (1982). Origin of high-magnesian andesites in the Setouchi volcanic belt southwest Japan, I. Petrological and chemical characteristics. *Earth and Planetary Science Letters* **60**, 293-304.

van Keken, P. E., Kiefer, B. & Peacock, S. M. (2002). High-resolution models of subduction zones: Implications for mineral dehydration reactions and the transport of water into the deep mantle. *Geochemistry Geophysics Geosystems* **3**, 1056, doi:10.1029/2001GC000256.

Wallace, P. J. (2005). Volatiles in subduction zone magmas: concentrations and fluxes based on melt inclusion and volcanic gas data. *Journal of Volcanology and Geothermal Research* **140**, 217-240, doi:10.1016/j.jvolgeores.2004.07.023.

Wallace, P. J. & Carmichael, I. S. E. (1999). Quaternary volcanism near the Valley of Mexico: implications for subduction zone magmatism and the effects of crustal thickness variations of primitive magma compositions. *Contributions to Mineralogy and Petrology* **135**, 291-314, doi:10.1007/s004100050513.

Wood, B. J. & Turner, S. P. (2009). Origin of primitive high-Mg andesite: Constraints from natural examples and experiments. *Earth and Planetary Science Letters* **283**, 59-66, doi:10.1016/j.epsl.2009.03.032.